Published as:
MacGowan, S. A.; Senge, M. O. (2013):
Computational Quantification of the Physicochemical Effects of Heme Distortion – Redox Control in the Reaction Center Cytochrome Subunit of *Blastochloris viridis.*
Inorganic Chemistry **52**, 1228–1237.

Computational Quantification of the Physicochemical Effects of Heme Distortion – Redox Control in the Reaction Center Cytochrome Subunit of *Blastochloris viridis*

*Stuart A. MacGowan and Mathias O. Senge**

School of Chemistry, SFI Tetrapyrrole Laboratory, Trinity Biomedical Sciences Institute, 152-160 Pearse Street, Trinity College Dublin, Dublin 2, Ireland

KEYWORDS: Hemeproteins, H-NOx, cytochromes, photosynthesis, reduction potential, crystal structures, DFT, structure-function correlation

ABSTRACT: A facile, experimentally calibrated computational procedure is described that affords the relative ordering of heme cofactor reduction potentials with respect to intrinsic shifts brought about by apoprotein induced heme-macrocycle distortion. The method utilizes heme-Fe partial atomic charges and is useful with the computationally inexpensive B3LYP/3-21g method calculated for simplified heme models extracted from the Protein Data Bank incorporating only the effects of varying macrocycle conformations and thereby delineating their physicochemical effects. The procedure was successfully calibrated using the atomic coordinates and published

mid-point potentials from the heme cofactors in wild-type and a series of heme-NO and $-O_2$ binding domain mutants and thus confirmed the sole conformational modulation of the redox potentials in these complexes. This technique was also applied to the reaction center tetraheme cytochrome subunit of *Blastochloris viridis* to build upon previous work elucidating the role that conformational control plays in photosynthetic systems and it was found that this effect may account for up to 70% (54mv) of the observed differences in the reduction potentials of the four hemes. We validate the approach using larger basis sets up to and including the triple-ζ, doubly polarized and augmented 6-311+g** basis and discuss the specific conformational origins of the effect.

INTRODUCTION

Hemeproteins and other tetrapyrrole containing biomolecules are one of the most diverse classes of enzymes present in the natural world.[1-4] Through recognition of the homologies of the active constituents of the globins, cytochromes and peroxidases (heme) as well as reaction centers and light-harvesting complexes (chlorophylls, bacteriochlorophylls, pheophytins) it is apparent that nature has evolved methods with which to utilize the same chemical cofactor for a range of disparate chemistries and enzymatic transformations, including electron transfer, small ligand binding, charge-separation and exciton transfer.[3, 5, 6] The plasticity of these cofactors with respect to physicochemical modulation in complexes is particularly emphasized by heme protein reduction potentials, which exhibit an impressive range spanning 1V from -550mV to +450mV versus SHE[7] and are a key-determinant of their biological functions[8]. As an addition to the classical concepts of apoprotein cofactor control *via* axial ligation, H-bonding and charged-residue electrostatic influences,[1, 8, 9] we have advocated the structural importance of the conformational flexibility of the porphyrin macrocycle as a modulator of cofactor properties and

function.[10] Here, we build upon this work by assessing the role of conformational control in modulating the reduction potentials of the hemes in the reaction center tetraheme cytochrome subunit of *Blastochloris viridis* (RC-CYT) through a combined statistical analysis of the heme conformations afforded by the available crystal structure data and subsequent application of an experimentally calibrated computational procedure.

Originally, the concept of conformational control arose from observations that the extended aromatic π-system of porphyrins was flexible with respect to distortion from planarity in structural studies on both synthetic and biological compounds that revealed the characteristic saddled, ruffled and domed macrocycle conformations.[11-14] The biological relevance of these observations was realized later when it was discovered that specific conformations were often conserved within particular enzyme classes.[15-18] This, considered with the knowledge that the distortions were found to alter (often systematically) chromophore absorption, redox and excited state behaviours,[12,19] provided an additional chemical rationale for the biological versatility of tetrapyrrole cofactors.

These physicochemical consequences of nonplanarity were deduced primarily from model compound studies which correlated increasing macrocycle distortion with bathochromic shifts of the UV/Vis Q-bands, easier oxidation and hindered reduction (for macrocycle centered redox processes) and decreasing S_1-lifetimes.[12,19,20] In contrast however, computational investigations of macrocycle nonplanarity experienced a period of inconsistency, sparking lively debate amongst experts and giving rise to such controversies as the publicized debunking of nonplanar physicochemical modulation in favor of the short-lived concept of In-Plane Nuclear Rearrangement.[21-24] This debate continued until specific flaws were identified in the structural models used and it was once again widely accepted that it is the distortions of the porphyrinoid

macrocycle that give rise to these effects.[22] Considering this historical development, an experimentally verifiable computational method for evaluating the physicochemical effects of macrocycle structural perturbation is a desirable goal which has not yet been fully realized.

In this later respect, our approach was enabled by the recent work of Olea *et al* where conformational control was used to impart redox modification through mutagenesis of the heme-NO and $–O_2$ binding domain (H-NOx) from *Thermoanaerobacter tengcongensis*.[25] They reported that the reduction potential of the H-NOx complex could be reduced *via* site-specific mutations that allowed the highly distorted heme cofactor to relax into a less nonplanar conformation. They also found that the decreased potentials were due to a measurable decrease of electron density at the heme-Fe as indicated by UV/Vis spectroscopy and the pK_as of the bound aqua ligands. Since this study controlled for any non-conformational influences by selecting residue substitutions that changed neither the H-bonding of the cofactor nor the local dielectric environment, it presented an ideal reference from which to establish a quantitative relationship between the macrocycle conformation and distortion induced potential shifts through calculable quantum mechanical properties of the isolated hemes.

With this relationship in hand, we continued our work regarding nature's exploitation of conformational control to enhance the efficiency of photosynthetic reaction centers and decided to assess the role macrocycle distortion plays in the modulation of the redox potentials of the individual hemes in the reaction center tetraheme cytochrome subunit of *B. viridis* (RC-CYT). This subunit is tethered to the reaction center in the periplasmic space above the membrane and serves the purpose of re-reducing the oxidized special-pair of the electron transfer chain (Figure 1).[26,27] The four hemes are grouped into pairs of low- and high-potential cofactors and these pairs are arranged such that a chain of alternating low/high redox potentials is created through to the

special-pair (*i.e.*, low, high, low, high, SP; Figure 1).[28,29] In this order, the individual hemes will be referred to here as H1, H2, H4 and H3, respectively (adopted from order of connection to the protein backbone). Previous studies regarding the factors responsible for controlling the hemes' *in situ* potentials have achieved accuracy to within ±25mV *via* electrostatic calculations, delineating the effects of charged residues in the vicinity of the heme, the protonation state of the heme propionates, the axial ligands of the heme-Fe and the inter-heme redox couplings but including only marginally the effects of the hemes' varying conformations.[30]

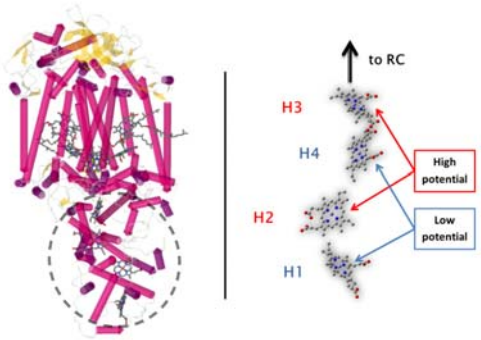

Figure 1. Illustration of the tetraheme cytochrome subunit in the reaction center of *B. viridis* (image adapted from the coordinates of PDB ID: 1PRC).

Since there are 15 crystal structures available from the PDB of the *B. viridis* reaction center, the question arises as to which one to select to perform the final part of our analysis? Our previous experience in this area suggests that standard quality metrics (*e.g.* resolutions, R-factors) for these large biomolecule crystal structures are not necessarily the decisive factor when one is interested solely with the detailed conformation of the cofactors.[10] Instead therefore, we opted to perform a statistical analysis of the resolved conformations from all of the crystal structures and in so doing were able to uncover, and somewhat characterize, latent experimental biases which resulted in three sets of mean cofactor conformations (*i.e.*, 12 heme structures) for our calculations.

To summarize, the focus of this paper is the proposal of a facile technique to predict and delineate the redox influence of macrocycle distortion in hemes and its application to further elucidate the role conformational control plays in the reaction center cytochrome subunit of *B. viridis*.

EXPERIMENTAL

Raw Data and NSD. The crystallographic atomic coordinates of the relevant H-NOx and RC-CYT hemes were obtained from the PDB Ligand Expo[31] and analyzed using the procedure of normal-coordinate structure decomposition (NSD)[32] in which the macrocycle conformation is described by a linear decomposition into a basis composed of the macrocycle's internal normal-modes of vibration. This basis may consist of either the full set of 66 (3N – 6) *normal-coordinates* or any given subset. In their original formulation, Jentzen *et al.* termed the full set the *complete basis* and suggested two other useful bases: the *minimum* and *extended basis*.[32] These reduced bases are composed of either the lowest-energy (min.) or the lowest- plus next-to-lowest-energy (ext.) normal-modes of each symmetry type. The utility of these reduced bases is that they yield a simplified analysis whilst their appropriateness is both allowed theoretically by the fact that the largest contributions to the observed conformations are expected to be distortions of relatively low energy and assessed practically by considering the root mean square deviation between the *simulated structure* (*i.e.* the conformation represented by the reduced basis) and the actual structure. Thus, NSD yields the magnitudes of each of the component normal-modes present in the chosen basis that contribute to the analyzed structure; a quantitative interpretation of the conformation. These data were used to determine the estimates of the RC-CYT heme conformations *via* a statistical analysis of the available crystal structures in a manor described in

detail previously[10] (see also below) and to construct the various cofactor models discussed used for the calculations.

Theoretical Method. The model structures used as inputs for the DFT calculations were selected so that the heme cofactor's structural parameters (*i.e.* substituent orientation, Fe-position, macrocycle conformation [including NSD reduced bases]) would be treated individually. The "diacid" model structures were formed by adding hydrogen atoms to the crystallographically resolved cofactor coordinates, adding the propionic acid proton to the oxygen with the longest C-O bond. The first Fe-porphin (FeP) model was also obtained directly from the crystal structure coordinates by replacing the macrocycle side-chains with hydrogen atoms. The "FeP-min, -ext and -comp" models were generated by projecting the relevant weighted normal-deformations (minimum, extended or complete, respectively) back onto the reference macrocycle in 3D-Cartesian space and by positioning the Fe-atom at the coordinate-system's origin (since the reference macrocycle is centrosymmetric about this point) thereby providing a reduced model that accounts only for the macrocycle normal-mode distortions alone, eliminating any possible macrocycle conformation/Fe-position interaction.

The quantum calculations were performed with the Gaussian 09[33] package using the facilities of the Trinity Centre for High-Performance Computing. The Fe-atom Mulliken[34] and minimal basis set Mulliken[35-36] atomic charges ($Q_{Fe\text{-}Mulk}$ and $Q_{Fe\text{-}mbs}$, respectively) of the heme models were obtained from single-point energy calculations using the B3LYP functional[37] and various basis sets. Natural atomic charges and orbital occupancies were obtained from Natural Population Analysis[38] using the NBO 3.1 implementation in Gaussian 09. In particular, we performed each calculation using the 3-21g,[39-40] 6-31g*, 6-311g**[41-44] and 6-311+g**[41-44] basis sets in order to roughly ascertain the parameters' basis set dependency and so to find an

appropriate balance between accuracy and expense. H-atom optimizations were not performed (to save on computational expense) as earlier trial computations (S.I. Figure 1) indicated that they had no bearing upon the resultant Mulliken charges compared to the default hydrogen atom addition parameters used by the GaussView[45] software for SP^2-carbons (*i.e.* d(C-H) = 1.07 Å and ∠(R1-C-H) = ∠(R2-C-H) = [360° - ∡(R1-C-R2)]/2 such that the added hydrogen is coplanar with the SP^2 center and its other directly bonded atoms).

Statistical Analysis of Cofactor Conformations. Analysis of the conformations of the RC-CYT hemes began with agglomerative hierarchical clustering (AHC) of each cofactor's minimum basis NSD in order to discover whether or not the crystal structure data were consistent with the hypothesis of distinct cofactor conformations. Thus, the AHC was performed on data matrices containing observations of the NSD minimum basis for each cofactor within the R statistical environment[46] using the Euclidean distance measure to build the dissimilarity matrix and Ward's method for the agglomeration.

The method of AHC was ideal for this purpose because it provides information relating to the similarity of observations based on any number of numerical variables. In detail, observations are algorithmically grouped together (clustered) based on their mutual (dis)similarity, calculated using a suitable distance metric; here, the Euclidean distance ($d_{i,j} = \sqrt{[\sum(x_{i,j} - x_{i,j})^2]}$). The decision as to how many clusters to select, between the extremes of one cluster containing all observations and as many clusters as there are observations, was achieved by consideration of the cluster dendrogram, which shows the interrelationships between possible clusters. For the agglomeration step, we used Ward's method which can be considered to agglomerate with respect to reducing the information loss at each step. Therefore in chemical terms, since we

clustered the NSD deformations of the cofactors, we obtained groups of cofactors that had similar resolved conformations.

In order to identify and isolate any systematic discrepancies between sets of structure determinations, the collected NSD data were then treated so that each PDB entry was considered as an individual observation and the minimum basis NSD deformations of its cofactors the observables. In detail, the data was formed into an *m x n* matrix where *m* is equal to the number of crystal structures included and *n*, the number of variables, equals the number of cofactors included (*i.e.* four hemes) multiplied by the number of NSD basis parameters used (*e.g.* B_{2u} of H1 is a distinct variable from B_{2u} of H2 and there is no categorical variable for cofactor identity). In the analyses of the experimental effects that followed, the 12 normal-coordinates of the minimum basis were used for each cofactor leading to a dataset of 15 observations of 48 variables. Application of both AHC and principal components analysis (PCA) to this data matrix allowed the crystal structures to be classified into groups exhibiting similar systematic errors (leaving only random fluctuations within each group) from which the mean conformations could be derived in the usual way.

Note that PCA, which here was used to complement AHC, is used to reduce the effective dimensionality of the data's variable space by forming linear combinations of the original variables termed the principle components (PCs) which account for as much variance, with as few PCs, as possible (*cf.* AHC which combines *observations*). Thus, here the PCs represent distortions along vectors made up of combinations of the normal-modes from the NSD analysis of the *four* cofactors in each structure and hence illustrate the influence of the structure determination *classification* (from the AHC) upon the resolved conformations.

RESULTS AND DISCUSSION

Calibration of a Computational Procedure for Evaluating Heme Conformational Control.

Initially, a number of computable parameters were tested in order to identify one which would correlate with the relative reduction potential shifts due to conformational control in the H-NOx WT, P115A, I5L and P115A/I5L complexes. The first attempt involved calculating standard estimates of the ionization potentials of the hemes in the form of HOMO (Koopmans' theorem) and ΔDFT ($E_{cation} - E_{neutral}$) energies; however, in these experiments no simple correlation with the observed trend in reduction potentials was found. Next, re-calling the electron deficiency that had been observed by Olea *et al*.[25] we thought it possible that this may be manifested in the Fe-atom partial atomic charges derived from atomic population analysis.

Thus, first the Fe-atom Mulliken atomic charges ($Q_{Fe\text{-}Mulk}$) were tested against the experimentally determined potentials (E_ms) of the H-NOx mutants where they provided, under certain conditions, strong, positive correlations. In particular, we found that $Q_{Fe\text{-}Mulk}$ from the singlet state B3LYP/3-21g wavefunctions correlated well with the H-NOx potentials (SI Figure 2A) but that the corresponding triplet state calculations resulted in $Q_{Fe\text{-}Mulk}$'s that showed only slight correlation (S.I. Figure 2B). Also, $Q_{Fe\text{-}Mulk}$'s obtained from any of the other basis-sets tested, in either state, provided poor correlations that often showed non-monotonic relations. Even though the strong correlation of the singlet state $Q_{Fe\text{-}Mulk}$ with the H-Nox E_ms appeared to satisfy our requirements, the lack of a good correlation with the equivalent triplet state partial-charges was worrisome since this state represented the ground state of our models (affording lower total energies (S.I. Tables 5-7) in accord with previous work on unligated Fe-porphins[47]) and furthermore, the failure to reproduce the correlation with the larger, more appropriate basis sets could lead to doubts regarding our causal interpretation of the result. These problems

necessitated further analysis and given the well-known numerical instability of Mulliken population analysis with respect to basis set size[48], we investigated alternative approaches.

The first of these was chosen to circumvent the basis set dependency of the Mulliken analysis directly, whilst retaining the remainder of the formalism. The method, known as minimum basis set Mulliken analysis (MBS) proceeds by projecting the MO-LCAO coefficients of the original basis onto those of a minimal basis and only thereafter performing the standard Mulliken analysis on these new MOs.[35-36] As hoped, the Fe-atom partial atomic charges obtained in this way ($Q_{Fe\text{-}MBS}$) provided remarkably improved correlations with the triplet state wavefunctions found using bases larger than 3-21g; confirming that the failures there were due to the basis sensitivity of Mulliken analysis and suggesting that the 3-21g basis was insufficient to reasonably describe the triplet structure. However, a few anomalous results were present. Specifically, irregular drops of either one of the 1U56 cofactors occurred using the 6-31g* basis with the diacid and FeP-ext. models as well as with the 6-311g** result for the FeP model. Also, non-monotonicity of $Q_{Fe\text{-}MBS}$ from the singlet calculations using the 6-31g* and 6-311g** bases was observed such that the former resulted in charges for the I5L (3NVR) cofactors that were less than those from I5L/P115A (3NVU), whilst the latter basis yielded $Q_{Fe\text{-}MBS}$ for I5L/P115A that were lower than the P115A (3EEE) structures (S.I. Figures X-X). On the other hand, progressively better correlations were obtained with increasing basis flexibility as may be expected for a truly causal, electronic relationship; gradual improvements observed for the triplet calculations and a discrete jump in agreement for the singlet state model with the 6-311+g** basis so much so that their respective calibration curves are statistically identical. With this in mind, the anomalies cited above should not represent any serious problem for our purpose since we are concerned primarily with the ground state (triplet) of the FeP-comp. model (as this

represents the best way to isolate fully the conformational influence) and are satisfied with the conclusion that the most flexible basis set employed here should be used to effect the most reliable results. Even so, for additional confirmation, we experimented with an entirely different form of population analysis, namely the Natural Poplation Analysis (NPA)[38].

Surprisingly, the Fe-atom partial charges obtained *via* NPA ($Q_{Fe\text{-}NPA}$) exhibited an *inverse* correlation with the H-NOx E_ms (S.I.), this being in contrast to the previous $Q_{Fe\text{-}MBS}$ / E_m trends, which were consistent with the experimental results from the H-NOx mutants (*vide supra*). Closer inspection warrantied, we found that this corresponded to an increase of both total valence and Rydberg Fe-atom natural orbital occupancies that overshadowed a decrease in the corresponding core orbital occupancies (S.I.). Although we are currently unable to rationalize and explain this phenomenon, and can find no other report of such inverse proportionality between these two methods in the literature, the strong empirical relationship, lack of anomalies for the 1U56 cofactors and reduced basis- and spin-state dependencies encouraged pursuit of NPA as a complementary approach, specifically using the Fe-core occupancy ($CORE_{Fe}$), not only because this parameter remained consistent with the previous findings and expectations, but also because it provided the best correlations (S.I.).

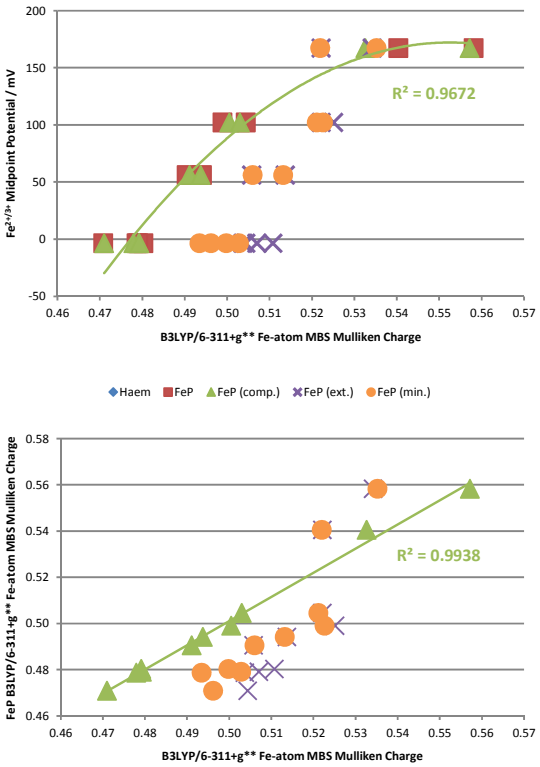

Figure 2. Plot of the measured $Fe^{2+/3+}$ midpoint potentials of the H-NOx mutants *versus* the calculated partial atomic charges of the heme-Fe ($Q_{Fe\text{-}MBS}$) from the various model structures in the singlet state (top) and correlation between $Q_{Fe\text{-}MBS}$ of the FeP model versus the other models of decreased complexity (bottom).

Turning now to the influence of the structural model used, the heme-diacid (not available for 6-311+g**), FeP and FeP-comp. triplet models provided very similar results (Figure 2, bottom), regardless of basis, emphasized by linear relations with gradients, intercepts and R^2 values within the ranges of 0.99-1.06; (-0.04)-0.00 and 0.98-1.00 for $Q_{Fe\text{-}MBS}$ (excluding the 1U56-B501 charge when outlying) and 0.89-1.07; (-1.22)-1.98 and 0.96-1.00 for $CORE_{Fe}$ (all results), respectively. These high values of R^2 confirm beyond doubt that it is purely the induced macrocycle conformation which is the cause of the potential shifts in these H-NOx mutants and that a

complex interaction between the macrocycle conformation and its side-chains, Fe-center, axial ligands and/or protein environment is not involved. We can comment also that the same behavior holds true for all of the structural models in the singlet state using the 3-21g basis, but we did not perform the full set of calculations for the remaining bases (only the FeP-comp. structures were assessed).

Additionally, the 2nd order polynomial fits for these models' central-Fe charges and core populations as explanatory variables for the mid-point shifts resulted in correlation coefficients all greater than 0.93 for the former (with the same exclusions outlined above) and 0.95 for the latter implying their suitability for interpolating the intrinsic potential shifts brought about by conformational control here and in other systems.

With respect to the effect of the structural model, the oversimplified FeP-min. and -ext. structures were only able to somewhat reproduce the relative experimental trends, especially with respect to the wild-type structure where the largest discrepancy, arising from heme 1U56 - B501, is the result of its resolved conformation, in which the minimum basis distortions are very much smaller than its counterpart in the asymmetric unit (Figure 3, note large error bars, and S.I. Table 21). However, the reasonable degree of linearity found within the results from the mutant complexes (*e.g.* $R^2 = 0.90$ for the linear relation between H-NOx E_m and the FeP-min. $CORE_{Fe}$ from the triplet calculations with the 6-311+g**) suggests that knowledge of the reduced basis NSDs may allow extraction of trend information, in the limit of low total distortion and with caution. This could be advantageous in situations where resolutions are poor (since low energy distortions are often larger than their higher energy counterparts and therefore easier to resolve), although for this to be possible it is clear that further work regarding the precise sensitivity of the

calculated parameters upon higher energy distortions is necessary before their application in quantitative work.

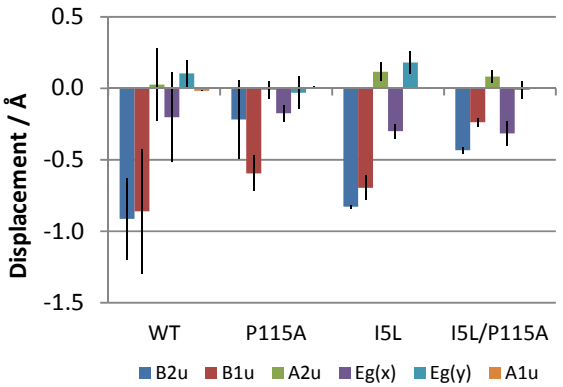

Figure 3. Mean out-of-plane minimum basis NSD of each heme from the H-NOx crystal structures used in the calibration. Error bars indicate two standard errors; PDBs 1U56, 3NVR and 3NVU, $n = 2$; 3EEE, $n = 4$ (hemes in asymmetric unit).

Another feature of the FeP-min. and -ext. models is that the more planar mutant structures exhibit a systematically greater calculated partial charge at the heme-Fe. This may be either a consequence of the lack of higher-energy distortions that correlate with those of lower-energies of the same symmetry or else the result of a subtler aspect of the NSD process itself, specifically that the reference macrocycle used for the in-plane deformation decomposition is a Cu-porphine,[32] which may mean that some higher-energy in-plane distortions are necessary to describe particular characteristic differences between this reference and an Fe-porphin. On the other hand, the systematically lower partial charges of the reduced basis models of the wild-type cofactors is most likely the result of the increasing dominance of the higher-energy distortion modes in affecting the molecular wavefunction and thus we suggest that it is the relationships between the distortions that is the cause of this behavior.

Derivation of Best Estimate(s) of Heme Conformations in *B. viridis* Cytochrome Subunit. The first task in elucidating the extent of conformational control in the RC-CYT subunit was to confirm that they possess distinct conformations with respect to one another. As previously shown,[10] and discussed in the experimental section, this can be achieved by agglomerative hierarchical clustering (AHC) of their NSDs. In this case, the clustering of the cofactors' NSDs was predominantly dependent upon the cofactor's identity which shows that the crystallographic experiments supported the hypothesis that each cofactor adopted a unique conformation (S.I. Figure 3). However, further consideration as to the composition of the clusters indicated that the H1 cofactors exhibited two distinct possible distortion patterns, a feature that was either related to two actual conformers or else to systematic differences between experiments (*i.e.* different systematic errors), in which the conformation of H1 is most affected. Since the previous experience has been that systematic differences can and do occur between multiple crystal structures of this type of macromolecule, which can be attributed to restraints during refinement,[10] and because cluster measurement appeared heavily dependent on the structure authors (S.I. Table 1), we investigated the possibility of the latter *via* analysis of the "structure-as-observation" data-matrix.

The dendrogram and evolution of the within cluster sum of squares from the AHC of the structure-as-observation matrix suggests that there are 2-4 meaningful clusters, within which the structures show similar trends for the conformations of the cofactors and between, they exhibit systematic variations (Figure 4, top and S.I. Figure 5). Furthermore, the correlation bi-plot from the PCA analysis of the systematic variations (Figure 4, bottom and see S.I. Figure 4 for scree-plot) shows that the greatest contributing variable to the systematic differences is the B_{2u} distortion of H1 and hence the bi-modal conformation of H1 noted above is in fact the greatest

discriminator between the structure classes. The next key variables are the B_{1u} distortions of the H1, H2 and H4 cofactors and it is these correlations that all but confirm that the differences between the structures are artefactual since there is no known reason for the conformations of the cofactors to be coupled in this way. Also notable is the significant dependence of PC1 on the A_{2u} mode which becomes increasingly apparent when the mean conformations of the clusters are considered (Figure 5; note relatively large A_{2u} distortion of SC2 cofactors and correlate with their positions in Figure 4 bi-plot [structures 5, 10 and 11]).

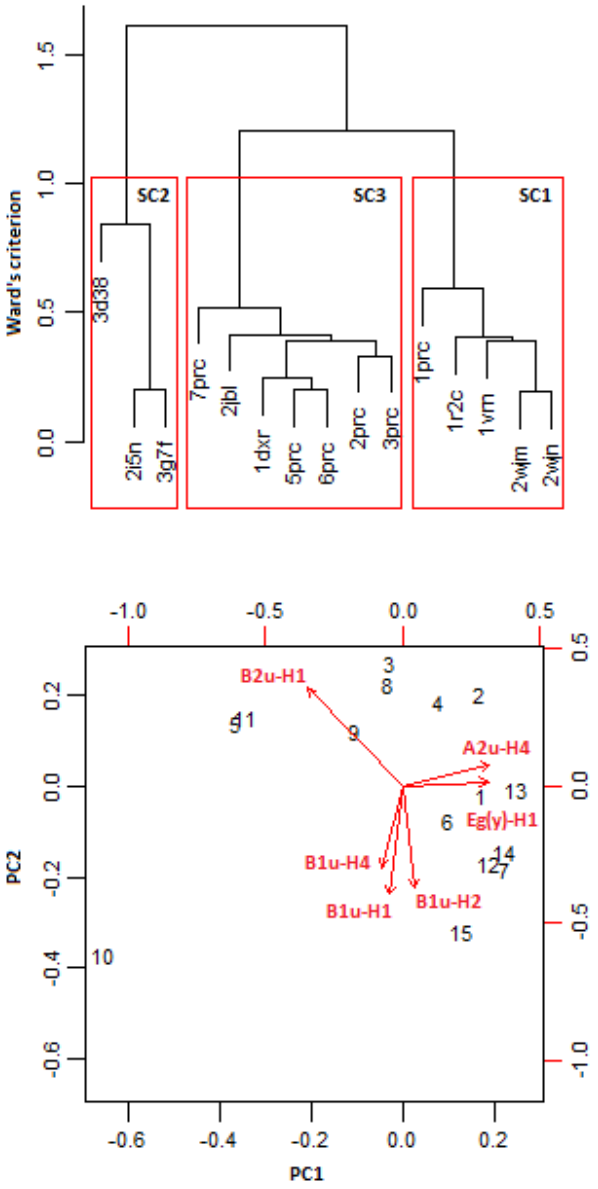

Figure 4. Dendrogram from the AHC of each PDB structures resolved minimum basis, out-of-plane NSDs of the four cofactors using the Euclidean metric and Ward's agglomeration (top; see S.I. Table 1 for structure key). Bi-plot from the PCA of the PDB structures' resolved minimum basis out-of-plane conformations of the four cofactors on the first two PCs and the top 25% correlating variables (bottom).

On the basis of this information we proceeded with a three cluster solution giving rise to three sets of mean conformations (Figure 5) highlighting the particular conformations of each cofactor and also confirming that the two apparent conformers of the H1 cofactor are largely characterized by the extent of the saddling (B_{2u} mode) of the macrocycle. In addition to this we see that, on the whole, the minimum basis distortions of the cofactors indicated by the means of SC1 (structure-cluster 1) and SC2 are in some ways more similar than those of SC3 (in contrast to the relationship indicated by the cluster hierarchy; Figure 4, top). Specifically, the saddling of H1 in SC1 and -2 is relatively large, whereas in SC3 it is similar across H1-H3 and the relative amount of saddling to ruffling (B_{1u}) across H1-H3 is more consistent between SC1 and -2 compared to SC3. However, the main feature that differentiates the SC2 cluster is the high-degree of doming (A_{2u}) compared to structure sets SC1 and SC3. In SC3 also, the conformations of the cofactors are more similar across the hemes possibly indicating a greater influence of refinement restraints which could be responsible for the lesser nonplanarity of its conformation for H1 (Figure 5).

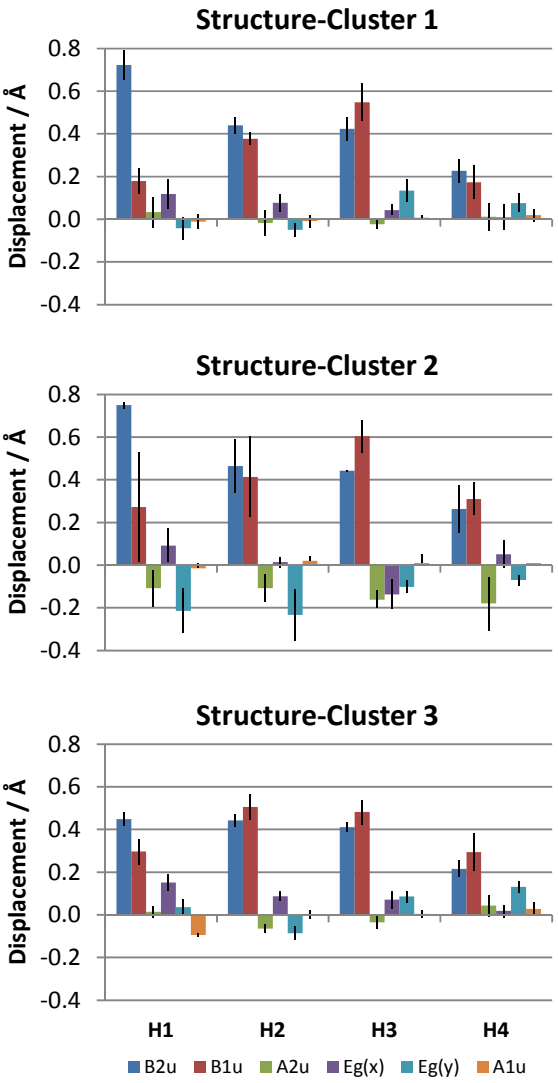

Figure 5. Mean out-of-plane minimum basis NSD of each heme cofactor from each cluster of crystal structures. Error bars indicate two standard errors. SC1 $n = 5$, SC2 $n = 3$ and SC3 $n = 7$.

Conformational Control in the *B. viridis* RC Cytochrome Subunit. Having established both a quantitative empirical relationship between the FeP-comp. models' triplet state B3LYP/6-311+g** Fe-atom MBS Mulliken atomic charges and the conformationally induced redox shifts, alongside the best estimate of the RC-CYT cofactors' conformations, we next sought to estimate the role of macrocycle mediated redox control in the RC-CYT.

Providing first a qualitative consideration of the particular structure-cluster results we see the SC1 structures' Fe-atom MBS Mulliken charges lie in the order H1 < H2 ≈ H3 << H4 implying that naturally evolved conformational control contributes to the observed low-potential of the H1 cofactor, the H2 > H1 potential difference, is consistent with the similar potentials of the H2 and H3 cofactors and in some way works to increase the potential of the H4 cofactor. Alternatively, SC2 yields $Q_{Fe\text{-}MBS}$ that vary so that H1 ≈ H2 < H3 ≈ H4 which corresponds with the fact that the H4/H3 low- and high-potential pair cofactors have systematically higher potentials than the corresponding H1/H2 pair. Finally, the SC3 conformations give $Q_{Fe\text{-}MBS}$ ordered H1 > H2 << H3 ≈ H4 which again corresponds with the observed larger potentials of the H4 and H3 pair but uniquely suggests that the conformational differences exerts influence to raise the H2 potential relative to H1. Whilst these results show clear differences between the inferred conformational effect, an emergent trend is clear; it seems that conformational control operates to raise the potentials of the H3/H4 pair relative to their counterparts (or conversely, to lower those of the H2/H1 pair). Before discussing this further however, we consider now the quantitative estimations of the distortion/redox influence.

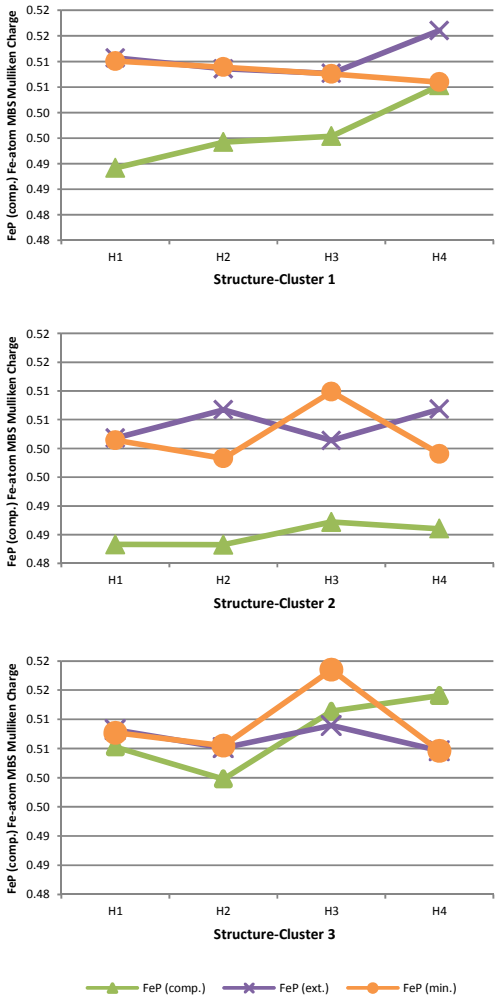

Figure 6. Fe-atom MBS Mulliken partial atomic charges ($Q_{Fe\text{-}MBS}$) calculated from mean FeP-comp., -ext. and -min. models of the three structure-cluster *B. viridis* RC-CYT hemes mean conformations in the triplet state with the B3LYP/6-311+g** method.

Noting that the RC-CYT Fe-atom MBS Mulliken charges (Figure 6), all fall within the range of interpolation from the H-NOx calibration (H-NOx FeP-comp 0.471037 – 0.557198e; RC-CYT H1-4 FeP-comp: SC1 0.489164 – 0.505313e; SC2 - 0.483259 – 0.487204e and SC3 - 0.499779 – 0.514082e) (FeP-comp: $E_m \approx -30440\ Q_{Fe}^2 + 33634\ Q_{Fe} - 9118.6$), we obtained the "H-NOx

potentials" (*vide infra*), allowing calculation of the relative potential shifts due to conformational control (Table 1).

In terms of a formal interpretation, if one considers that the reduction potential of a heme in a protein complex arises from a combination of perturbations effected by the environment relative to a free heme (reference) in solution, then the potential may be written as a sum of the reference potential and the perturbation as,

$$E_m^{complex} = E_m^{solution} + \Delta E_m^{perturbation}$$

where the last term is a sum of the contributions from all environmental considerations such as H-bonding, electrostatics, axial-ligands (if different from the reference), solvent accessibility and conformational control. In our case, since we are interested solely in delineating the effect of conformational control we may write this as,

$$E_m^{H-NOx} = E_m^{solution} + \Delta E_m^{H-NOx(environment)} + \Delta E_m^{conformation}$$

then, since the H-NOx series of complexes investigated varied solely in the last term, taking the difference of any two of their potentials yields exclusively the change in this component,

$$\Delta E_m^{H-NOx} = \Delta\left(\Delta E_m^{conformation}\right).$$

Consequently, taking the difference of any two interpolated "H-NOx potentials" (the potential that the H-NOx complex would exhibit if the heme within adopted the conformation of interest), yields the potential difference effected by their conformational difference.

The one possible caveat to this approach is that the extension of the H-NOx relationship to other proteins is dependent on whether or not the magnitude of the intrinsic potential shift brought about by macrocycle distortion is sensitive to the *specific* environment of the cofactor. Since there is no suggestion in the literature to the contrary we proceed to investigate the impact

of conformational control on the *B. viridis* hemes under the assumption that there is no such effect, although it must be noted that it is certainly possible that there are such differences.

The tabulated data below show the experimental and most recent, state-of-the-art, theoretically calculated cofactor potential shifts together with the estimated influence of conformational control obtained from our highest level calculation (B3LYP/6-311+g**). The interpretation of the entries in the middle of the non-experimental data correspond to the percentage of the difference accounted for by the quoted method, *e.g.* Voigt and Knapp's method accounted for 48% (36mV) of the H1-H4 difference whilst our method suggests that 72% (54mV) of the difference is due to conformational control.

Table 1. Absolute differences [$D_{i,j} = H_j - H_i$] and relative differences to experiment [$D_{i,j} = (H_j - H_i)_{calc}/(H_j - H_i)_{expt}$] of the heme midpoint potentials derived from the average of the two published experimental measurements; Voigt and Kanpp's potentials of the *B. viridis* hemes and of calculated Em(H-NOx) of the *B. viridis* hemes derived from $Q_{Fe\text{-}MBS}$ obtained from the triplet state B3LYP/6-311+g** wavefunctions of the FeP-comp. models. The third main column provides the experimental errors of the Voigt and Knapp model and of this model combined with the various structure-cluster estimates whilst the fourth shows the error differences that this brings about.

		Cofactor potential differences / mV				Expt. correlation				Expt. error of model + Voigt & Knapp				Change in absolute expt. error of model			
		H1	H2	H3	H4	H1	H2	H3	H4	H1	H2	H3	H4	H1	H2	H3	H4
Expt.	H1	0	365	435	75												
average[28-29]	H2	-365	0	70	-290												
	H3	-435	-70	0	-360												
	H4	-75	290	360	0												
Voigt &	H1	0	348	395	36		0.95	0.91	0.48		-17	-40	-39				
Knapp[30]	H2	-348	0	47	-312			0.67	1.08			-23	-22				
	H3	-395	-47	0	-359				1.00				1				

		Cofactor potential differences / mV				Expt. correlation				Expt. error of model + Voigt & Knapp				Change in absolute expt. error of model			
		H1	H2	H3	H4	H1	H2	H3	H4	H1	H2	H3	H4	H1	H2	H3	H4
	H4	-36	312	359	0												
SC1	H1	0	19	23	54		0.05	0.05	0.72		2	-17	15		-15	-23	-24
	H2	-19	0	4	36			0.06	-0.12			-19	14			-4	-8
	H3	-23	-4	0	32				-0.09				33				32
	H4	-54	-36	-32	0												
SC2	H1	0	0	16	11		0.00	0.04	0.15		-17	-24	-28		0	-16	-11
	H2	0	0	16	11			0.23	-0.04			-7	-11			-16	-11
	H3	-16	-16	0	-5				0.01				-4				3
	H4	-11	-11	5	0												
SC3	H1	0	-17	16	23		-0.05	0.04	0.31		-34	-24	-16		17	-16	-23
	H2	17	0	33	40			0.47	-0.14			10	18			-13	-4
	H3	-16	-33	0	7				-0.02				8				7
	H4	-23	-40	-7	0												

In most cases, the calculated perturbation of conformational control affects a change in potential that acts in concert with the other modulatory methods of the binding-site to increase the potential difference between cofactors (*i.e.* has the same sign as the experimental difference), except for H4 relative to both H2 and H3. Indeed it is notable that the H4-H2 difference is the only one which Voigt and Knapp's method overestimated, whilst that of H4-H3 is the only one that was not underestimated (the near exact agreement of their value for this difference is due in fact to a systematic error of around -30mV in both the H3 and H4 absolute potentials). Furthermore, the two largest potential differences due to conformational control as inferred from any one of the three sets of mean conformations are found to involve the H3 or H4 potentials with those of H2 or H1 (respectively) such that the potentials of the former are raised relative to the latter (Table 1).

It is convenient to assess the quantitative implications of our work in the context of improving the current theoretical understanding of the factors affecting the heme potentials by combining the Voigt and Knapp estimates of the inter-heme potential differences with any one of our estimates of the influence of conformational control. This should be deemed acceptable under the assumption that those previous theoretical estimates were precisely lacking this effect and because our isolation of it is total. Importantly, doing so provides significantly improved experimental agreement (RMSDs = 27mV for Voigt and Knapp, and 19mV, 17mV and 20mV after including the estimated conformational effect from mean conformations SC1, SC2 and SC3, respectively). Furthermore, considering the individual corrections, it is clear that the SC1 structures' derived shifts may well provide an even greater improvement to the absolute potentials than is implied by the reduction of the RMSD experimental agreement of the inter-heme relative differences because these results break the effect of Voigt and Knapp's systematic error for the H3 and H4 cofactors, if we were able to determine these soundly.

Whilst we have already suggested that the H1 conformation of SC3 may be less reliable from the structure-determination point of view, a pragmatic view of these results also suggests that this may be an erroneous result. This point is taken simply from the observed experimental disagreement of the predicted relative cofactor potential differences, the H1-H2 difference, which was already underestimated, is even more worse off with SC3's contribution and there is no systematic error in the theoretical potentials for these as there was with the H3-H4 cofactors (see above).

Conformational Origin of Haem Redox Modulation. A key feature that we have not yet discussed is that in the *B. viridis* cytochrome subunit, it is the cofactor with the *lowest* total nonplanar distortion (H4, Figures 5 and 6) that exhibits a consistently high relative partial charge

and that the cofactor with the *greatest* distortion exhibits one of the *lowest* charges (H1), which is in stark contrast to the situation in the H-NOx complex. Thus, it appears that the redox influence of the cofactor conformations is inverted between the two complexes. In order to begin to explain the origin of this phenomenon, we are required to investigate the correlations between the macrocycle modes of distortion and the calculated population parameters. The following discussion relates to our preliminary results only as, in general, the derivation of a logical relationship between heme conformation and electronic properties is a complicated endeavor and indeed one of our long term goals.

Combining the H-NOx and cytochrome data and regressing the heme-Fe MBS Mulliken charges and NPA core populations against the individual NSD parameters revealed one candidate above all others as the main indicator of the electronic population at the metal center, namely the A_{1g} or *breathing* mode. The extent of this distortion provided statistically significant correlation coefficients of 0.87 and 0.94 with the minimum basis cofactor projections and the corresponding $Q_{Fe\text{-}MBS}$ and $CORE_{Fe}$ values and, 0.78 and 0.83 for the complete basis projections (observed macrocycle conformation, centered Fe) and corresponding parameters. Furthermore, because this normal-mode represents most closely the actual macrocycle core size, and thus the Fe-N bond lengths, this behavior is perfectly understandable. We must highlight here that this result does not render the nonplanar macrocycle distortions as superfluous or secondary next to the in-plane conformation, as the outmoded concept of In-plane Nuclear Rearrangement, alluded to in the introduction, attempted to. Rather, multicollinearities are present between the various normal-coordinates that suggest that the A_{1g} distortion is *determined* by the nonplanar distortions and thus provides a conduit with which the nonplanar conformation exerts the real influence. Indeed, this structural relationship has been known for many years[22] and is supported by our own

semi-empirical calculations that find non-zero minima along the A_{1g} coordinate for arbitrarily imposed nonplanar distortions upon a previously optimized structure[S1].

However, this analysis provides only explicit investigation of the global situation, *i.e.* the source of conformationally induced potential shifts over a range of 171mV and two distinct complexes (for one of which we had three sets of possible, systematically different structure determinations) whilst our maximum estimated effect of natural conformational control in the cytochrome was only 54mV. Also, a perusal of the in-plane distortions of the *B. viridis* hemes (S.I.) suggested that whilst some of the variation appeared to correspond with the A_{1g} coordinate (in particular, the systematic lowering of the SC2 charges), this was by no means a conclusive resolution. Therefore, although at the expense of statistical sample size, to assess the situation in more detail we assessed the NSD/population parameter relations arising from meaningful subsets directly. Specifically, we additionally regressed subsets of the data comprised from the H-NOx structures, the H-NOx mutants only (105mV range), the H-NOx P115A and I5L/P115A mutants (60mV range) the *B. viridis* mean conformations and the individual structure-clusters of the latter.

Not unexpectedly, all but the largest of these subsets were too small to produce any *strictly* statistically significant correlations after alphas were adjusted for multiple comparisons. On the other hand, the results do suggest that the full set of A_{1g} modes may contribute to a considerable portion of the within group population variations. Nevertheless, even if these correlated in-plane distortions do provide the connection between the observed effects in each complex, it would then suggest that the nonplanarity induced contraction is reversed so that *expansion* occurs with increasing distortion.

There is however, a potential explanation for some of these observations. The first step is to understand most likely it is the *ruffle* distortion that results in the greatest core contraction, as it is known to do so for Ni-porphyrins[22] and on this basis we can somewhat account for the H1-H3 Fe populations. Next, having only to account for the high-partial charge of H4 we consider that the bis-HIS coordination of this heme that effects a large drop in its reduction potential and a corresponding increased Fe atom electron density it is possible then that the macrocycle contracts in order to stabilize this extra density.

However, it may have to suffice to say that it is the particular conformation that determines the metal population and the consequent conformational contribution to the redox potential although it appears clear that the satisfactory experimental agreement afforded by our method implies that it is fully capable of accounting for this fact.

CONCLUSIONS

By applying chemical intuition in an attempt to obtain an experimentally calibrated computational procedure with which to predict and delineate the influence of protein-induced macrocycle distortion upon heme reduction potentials, a strong correlation between heme-Fe MBS Mulliken atomic charges obtained using B3LYP wave functions with minimal- to triple-ζ, doubly polarized augmented basis sets and the redox potentials of intact complexes could be established, in the circumstance that the heme conformation was the only substantially varying property. This relationship will assist future research in the realm of naturally occurring conformational control and with further development may also prove useful for the design and tuning of heme enzymes where conformational change from residue mutations could be predicted using standard geometry optimizations and, from the resultant cofactor conformation,

the mutation's consequent physicochemical effect which could potentially reduce the cost and effort required to engineer proteins with desired redox properties.

Using this relationship together with the derivation of the best currently available estimates of the conformations' of the heme cofactors in the reaction center tetraheme cytochrome subunit of *Blastochloris viridis*, it was found that conformational control may account for up to 70% (54mV) of a particular potential difference. The estimated influence upon the reduction potentials of H1-3 appear to work concertedly with other protein influences to enhance the differences between them, whilst for H4 it significantly reduces effects of bis-HIS coordination[26,27] and the partial ionization of its propionates[30]. This shows that explicit consideration of the conformational contribution to heme reduction potential modulation *in situ* may provide a missing link with respect to understanding heme potential variability in general.

ASSOCIATED CONTENT

Supporting Information

Additional figures and tables that are referenced in text: comparison of heme-Fe Mulliken atomic charges obtained with and without peripheral H-atom optimization, heme-Fe Mulliken charges from triplet calculations, cluster hierarchy and composition from AHC of cofactor NSDs from all PDB entries, scree-plots from statistical analyses, PDB entry structure authorship, resolutions, references and key for figure 4, multivariate analysis of heme-Fe Mulliken charges obtained from individual cofactor coordinates. Tabulated data: all data-values presented in charts, DFT-SCF energies, heavy-atom coordinates for models of reduced complexity, all cofactor minimum basis NSDs. Complete author list for reference 33. This material is available free of charge via the Internet at http://pubs.acs.org.

AUTHOR INFORMATION

Corresponding Author

*E-mail: sengem@tcd.ie

Notes

The authors declare no competing financial interest.

ACKNOWLEDGEMENTS

This work was supported by Science Foundation Ireland (SFI P.I. 09/IN.1/B2650). All calculations were performed on the Lonsdale cluster maintained by the Trinity Centre for High Performance Computing. This cluster was funded through grants from Science Foundation Ireland.

ABBRIEVIATIONS

AHC, agglomerative hierarchical clustering; H-NOx, heme-NO and $-O_2$ binding domain; NSD, Normal-coordinate structural decomposition; PCA, principal components analysis; PDB, Protein Data Bank; RC-CYT, reaction center cytochrome subunit; SC(1-3), structure-clusters 1-3; SHE, standard hydrogen electrode.

REFERENCES

1. Chapman, S. K.; Daff, S.; Munro, A. W. Heme: The most versatile redox centre in biology? In *Structure and Bonding*, Hill, H., Sadler, P. J., Thomson, A., Eds.; Springer: Berlin, **1997**, Vol. 88, pp 39–70

2. Poulos, T.L. *Nat. Prod. Rep*. **2007**, *24*, 504-10.

3. Bertini, I.; Cavallaro, G.; Rosato, A. *Chem. Rev.* **2006**, *106*, 90–115.

4. Reedy, C. J.; Gibney, B. R. *Chem. Rev.* **2004**, *104*, 617–50.

5. Rodgers, K. R. *Curr. Opin. Chem. Biol.* **1999**, 3, 158-67.

6. Breton, J.; Martin, J. -L.; Migus, A.; Antonetti, A.; Orszag, A. *Proc. Natl. Acad. Sci. USA* **1986**, *83*, 5121-5.

7. Reedy, C. J.; Elvekrog, M. M.; Gibney, B. R. *Nucleic Acids Res.* **2008**, *36*, D307-13.

8. Zheng, Z.; Gunner, M. R. *Proteins* **2009**, *75*, 719-34.

9. Allen, J. P.; Williams, J. C. The Influence of Protein Interactions on the Properties of the Bacteriochlorophyll Dimer in Reaction Centers. In *Adv. Photosynth. Respir.*; Grimm, B., Porra, R. J., Rudiger, W., Scheer, H., Eds.; Springer: Dordrecht, **2006**, Vol. 25, 283-95.

10. MacGowan, S. A.; Senge, M. O. *Chem. Commun.* **2011**, *47*, 11621-3.

11. Senge, M. O. Highly Substituted Porphyrins. In *The Porphyrin Handbook*; Smith, K. M., Kadish, K. M., Guilard, R., Eds.; Academic Press: San Diego, **2000**; Vol. 1, pp 239-347.

12. Senge, M. O. *Chem. Commun.* **2006**, 243-56.

13. Scheidt, W. R.; Reed, C. A. *Chem. Rev.* **1981**, *81*, 543-55.

14. Kratky, C.; Waditschatka, R.; Angst, C.; Johansen, J. E.; Plaquevent, J. C.; Schreiber, J.; Eschenmoser, A. *Helv. Chim. Acta* **1985**, *68*, 1312-38.

15. Hobbs, J. D.; Shelnutt, J. A. *J. Prot. Chem.* **1995**, *14*, 19-25.

16. Jentzen, W.; Ma, J. G.; Shelnutt, J. A. *Biophys. J.* **1998**, *74*, 753-63.

17. Senge, M. O. *J. Photochem. Photobiol. B* **1992**, *16*, 3-36.

18. Fajer, J. *Isr. J. Chem.* **1992**, *32*, 363-518.

19. Röder, B.; Büchner, M.; Rückmann, I.; Senge, M. O. *Photochem. Photobiol. Sci.* **2010**, *9*, 1152-8.

20. Senge, M. O.; Renner, M. W.; Kalisch, W. W.; Fajer, J. *Dalton Trans.* **2000**, 381-5.

21. Ryeng, H.; Ghosh, A. *J. Am. Chem. Soc.* **2002**, *124*, 8099-103.

22. Haddad, R. E.; Gazeau, S.; Pecaut, J.; Marchon, J. C.; Medforth, C. J.; Shelnutt, J. A. *J. Am. Chem. Soc.* **2003**, *125*, 1253-68.

23. Dimagno, S. G.; Wertsching, A. K.; Ross, C. R. *J. Am. Chem. Soc.* **1995**, *117*, 8279-80.

24. Wertsching, A. K.; Koch, A. S.; DiMagno, S. G. *J. Am. Chem. Soc.* **2001**, *123*, 3932-9.

25. Olea, C., Jr.; Kuriyan, J.; Marletta, M. A. *J. Am. Chem. Soc.* **2010**, *132*, 12794-5.

26. Deisenhofer, J.; Epp, O.; Miki, K.; Huber, R.; Michel, H. *Nature* **1985**, *318*, 618-24.

27. Deisenhofer, J.; Epp, O.; Miki, K.; Huber, R.; Michel, H. *J. Mol. Biol.* **1984**, *180*, 385-98.

28. Dracheva, S. M.; Drachev, L. A.; Konstantinov, A. A.; Semenov, A.; Skulachev, V. P.; Arutjunjan, A. M.; Shuvalov, V. A.; Zaberezhnaya, S. M. *FEBS J.* **1988**, *171*, 253-64.

29. Fritzsch, G.; Buchanan, S.; Michel, H. *Acta Biochim. Biophys.* **1989**, *977*, 157-62.

30. Voigt, P.; Knapp, E. W., *J. Biol. Chem.* **2003**, *278*, 51993-2001.

31. Feng, Z.; Chen, L.; Maddula, H.; Akcan, O.; Oughtred, R.; Berman, H. M.; Westbrook, J. *Bioinformatics* **2004**, *20*, 2153-5.

32. Jentzen, W.; Song, X. Z.; Shelnutt, J. A. *J. Phys. Chem. B* **1997**, *101*, 1684-99.

33. Frisch, M. J. et al. *Gaussian 09 Revision A. 02*, Gaussian, Inc. Wallingford CT, **2009**.

34. Mulliken, R. S. *J. Chem. Phys*. **1955**, *23*, 1833-40.

35. Montgomery Jr., J. A.; Frisch, M. J.; Ochterski, J. W.; Petersson, G. A. *J. Chem. Phys.* **2000**, *112*, 6532-42.

36. Montgomery Jr., J. A.; Frisch, M. J.; Ochterski, J. W.; Petersson, G. A. *J. Chem. Phys.* **1999**, *110*, 2822-7.

37. Becke, A. D. *J. Chem. Phys.* **1993**, *98*, 5648-52.

38. Reed, A. E.; Weinstock, R. B.; Weinhold, F. *J. Chem. Phys.* **1985**, *83*, 735-46.

39. Binkley, J. S.; Pople, J. A.; Hehre, W. J. *J. Am. Chem. Soc.***1980**, *102*, 939-47.

40. Dobbs, K. D.; Hehre, W. J. *J. Comp. Chem.* **1987**, *8*, 861-79.

41. Raghavachari, K.; Binkley, J. S.; Seeger, R.; Pople, J. A. *J. Chem. Phys.* **1980**, *72*, 650-4.

42. Wachters, A. J. H. *J. Chem. Phys.* **1970**, *52*, 1033.

43. Hay, P. J. *J. Chem. Phys.* **1977**, *66*, 4377-84.

44. Raghavachari, K.; Trucks, G. W. *J. Chem. Phys.* **1989**, *91*, 1062-5.

45. Dennington, R.; Keith, T.; Millam, J. *GaussView Version 5*, Semichem Inc. Shawnee Mission KS, **2009**.

46. R Development Core Team *R: A language and environment for statistical computing* R Foundation for Statistical Computing Vienna, Austria, **2010**.

47. Rovira, C.; Kunc, K.; Hutter, J.; Ballone, P.; Parrinello, M. *J. Phys. Chem. A* **1997**, *101*, 8914-25.

48. Liu, W.; Li, L. *Theor. Chem. Acc.* **1997**, *95*, 81-95.

49. MacGowan, S. A.; Senge, M. O. *unpublished results*.

Table of Contents Graphic and Synopsis

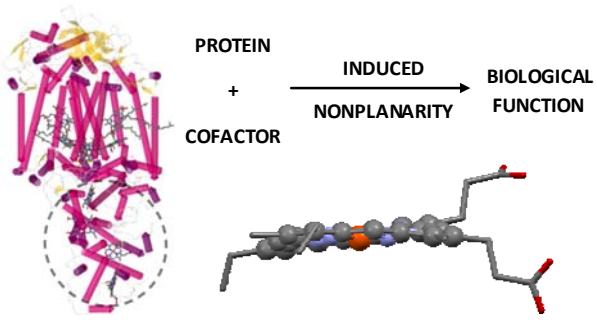

A facile, experimentally calibrated computational procedure is described that affords the relative ordering of heme cofactor reduction potentials with respect to intrinsic shifts brought about by apoprotein induced heme-macrocycle distortion. This technique was applied to the reaction center tetraheme cytochrome subunit of *Blastochloris viridis* and it was found that conformational control may account for up to 70% (54mV) of the observed variation in the reduction potentials of the four hemes.

Supplementary Information

Computational Quantification of the Physicochemical Effects of Heme Distortion – Redox Control in the Reaction Center Cytochrome Subunit of Blastochloris Viridis

Stuart A. MacGowan and Mathias O. Senge

Contents

Additional Information

Comparison of computational methods for H-atom optimisation

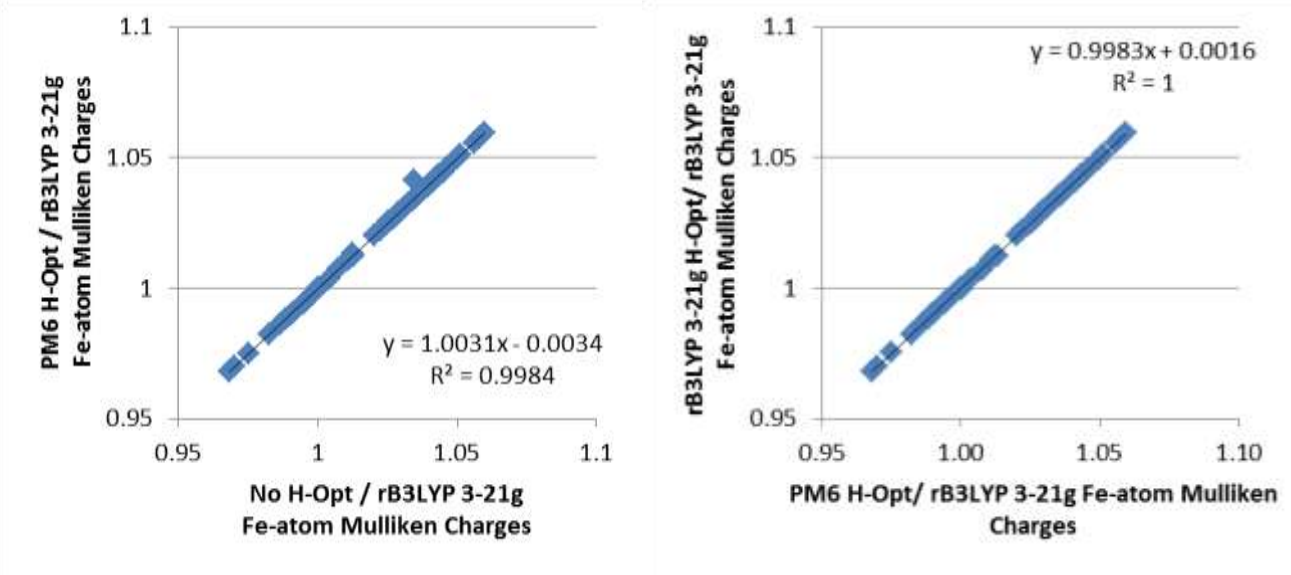

Figure 1: Comparison of Fe-atom Mulliken charges obtained from B3LYP/3-21g single-point energies with different methods of H-atom optimisation for the input structures.

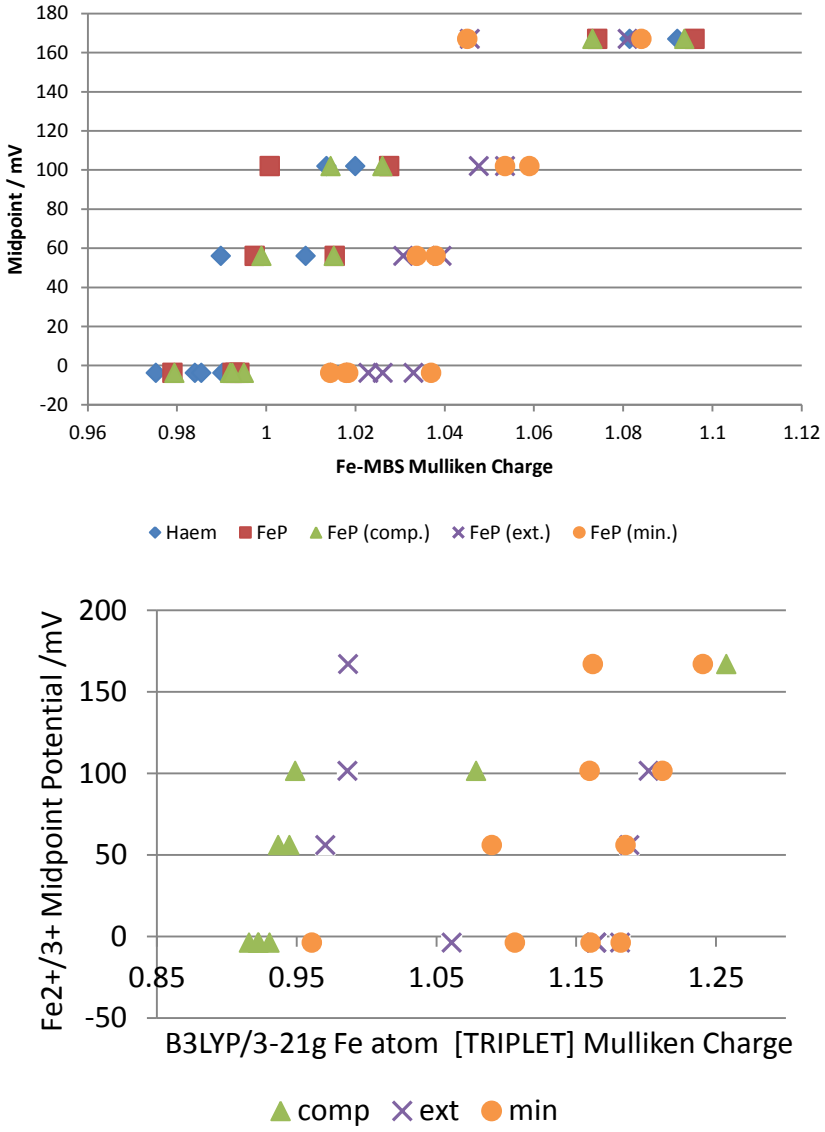

Figure 2: Plot of the measured Fe2+/3+ midpoint potentials of the H-NOX mutants versus the calculated partial atomic charges of the haem-Fe from the various models in the singlet- (top) triplet state (bottom).

Distinctness of Conformations

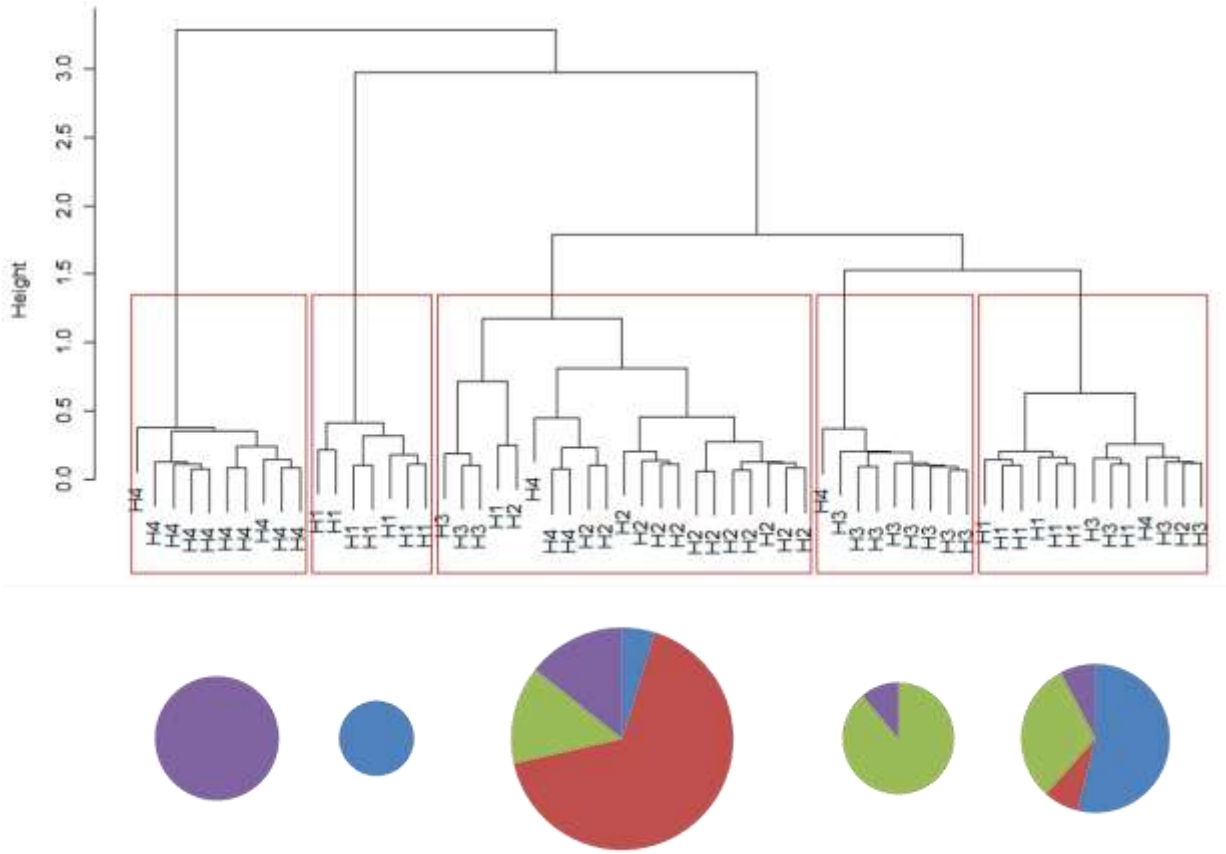

Figure 3: Dendrogram from the AHC of the cofactors' minimum basis, out-of-plane NSDs using the Euclidean metric and Ward's agglomeration. Pie-charts show proportion of each cofactor in the rectangled cluster above it; blue = H1, red = H2, green = H3 and purple = H4. Note presence of two distinct clusters predominantly composed of cofactor H1.

Investigation of Variance of Systematic Error

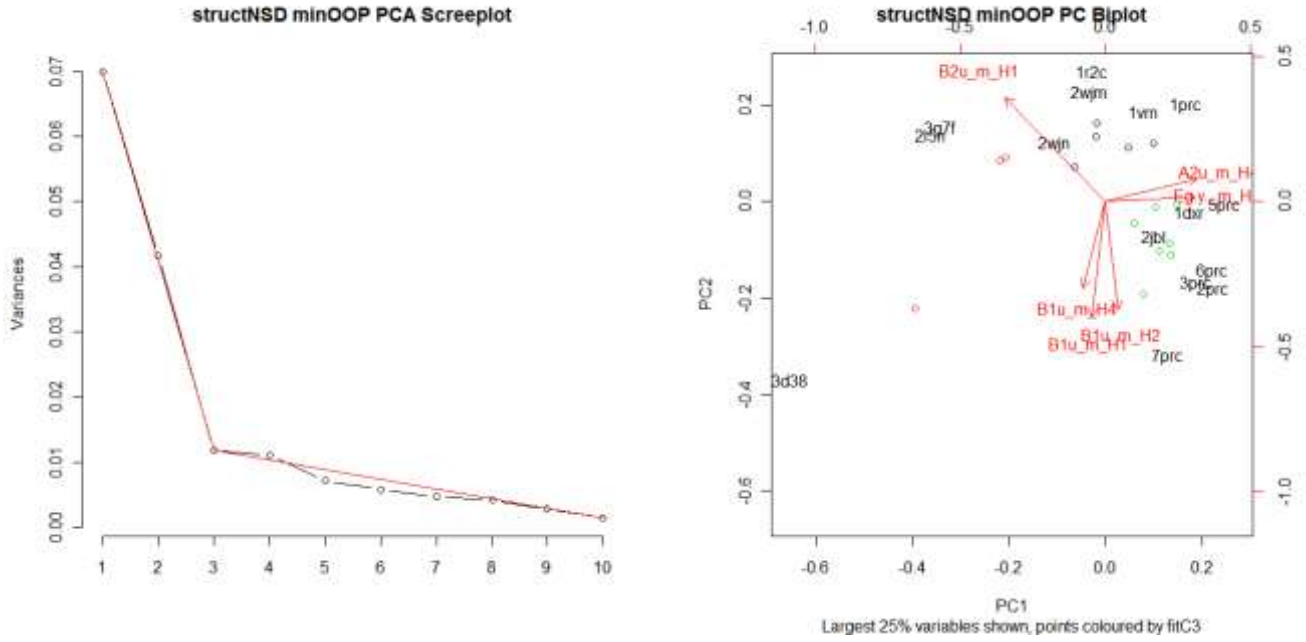

Figure 4: Scree-plot from the PCA of the PDB structures' resolved minimum basis out-of-plane conformations for the four cofactors; note elbow at 3 principal components which indicates either 2 or 3 significant PCs (left) and the corresponding bi-plot of the first two PCs showing only the top 25% correlating variables (right).

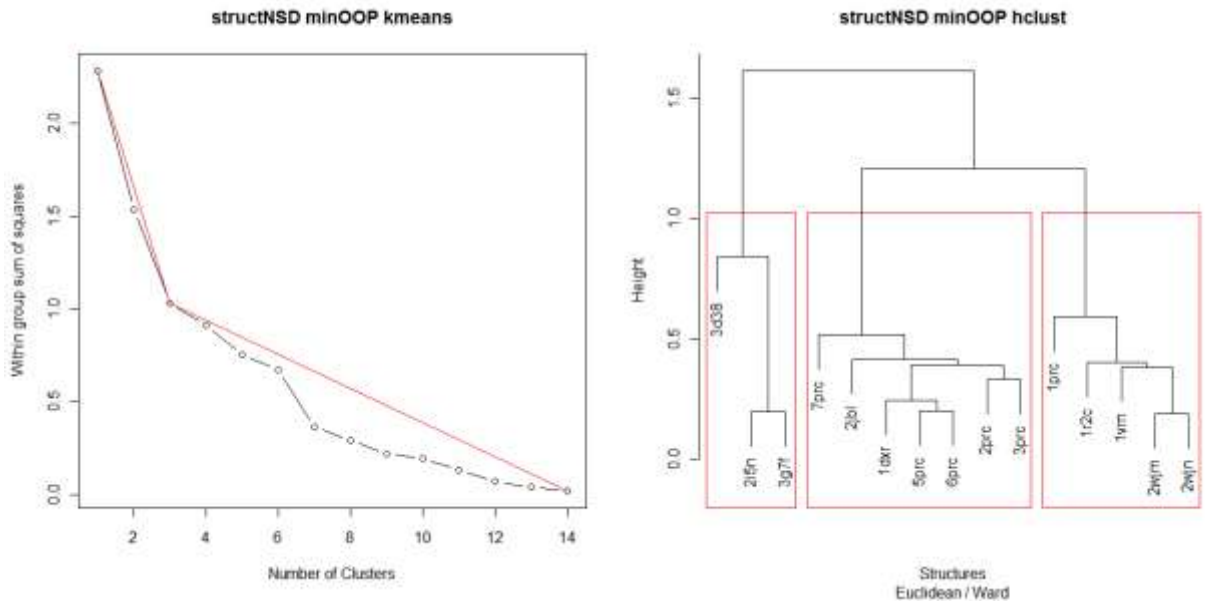

Figure 5: Plot of the within group sum of squares as a function of number of clusters from kmeans analysis of the structures' resolved minimum basis out-of-plane conformations for the four cofactors (left). Dendrogram from the AHC of each PDB structures resolved minimum basis, out-of-plane NSDs of the four cofactors using the Euclidean metric and Ward's agglomeration (right).

Table 1: Basic PDB structure information regarding the *B. viridis* RC crystal structures organised according to structure-cluster membership.

Cluster	PDB	Structure Authors	Res.	Fig. 4	Ref.
SC2	3d38	Li, L., Nachtergaele, S.H.M., Seddon, A.M., Tereshko, V., Ponomarenko, N., Ismagilov, R.F.	3.21	10	[9]
	2i5n	Li, L., Mustafi, D., Fu, Q., Tereshko, V., Chen, D.L., Tice, J.D., Ismagilov, R.F.	1.96	5	[5]
	3g7f	Ponomarenko, N.S., Li, L., Tereshko, V., Ismagilov, R.F., Norris Jr., J.R.	2.50	11	[10]
SC3	7prc	Lancaster, C.R.D., Michel, H.	2.65	15	[11]
	2jbl	Lancaster, C.R.D.	2.40	6	[6]
	1dxr	Lancaster, C.R.D., Bibikova, M., Sabatino, P., Oesterhelt, D., Michel, H.	2.00	1	[1]
	5prc	Lancaster, C.R.D., Michel, H.	2.35	13	[11]
	6prc	Lancaster, C.R.D., Michel, H.	2.30	14	[7]
	2prc	Lancaster, C.R.D., Michel, H.	2.45	7	[7]
	3prc	Lancaster, C.R.D., Michel, H.	2.40	12	[11]
SC1	1prc	Deisenhofer, J., Epp, O., Miki, K., Huber, R., Michel, H.	2.30	2	[2]
	1r2c	Baxter, R.H., Ponomarenko, N., Pahl, R., Srajer, V., Moffat, K., Norris, J.R.	2.86	3	[3]
	1vrn	Baxter, R.H.G., Seagle, B.-L., Norris, J.R.	2.20	4	[4]
	2wjm	Woehri, A.B., Wahlgren, W.Y., Malmerberg, E., Johansson, L.C., Neutze, R., Katona, G.	1.95	8	[8]
	2wjn	Wohri, A.B., Wahlgren, W.Y., Malmerberg, E., Johansson, L.C., Neutze, R., Katona, G.	1.86	9	[8]

Propagation of Coordinate Error into Fe-atom Mulliken Charges

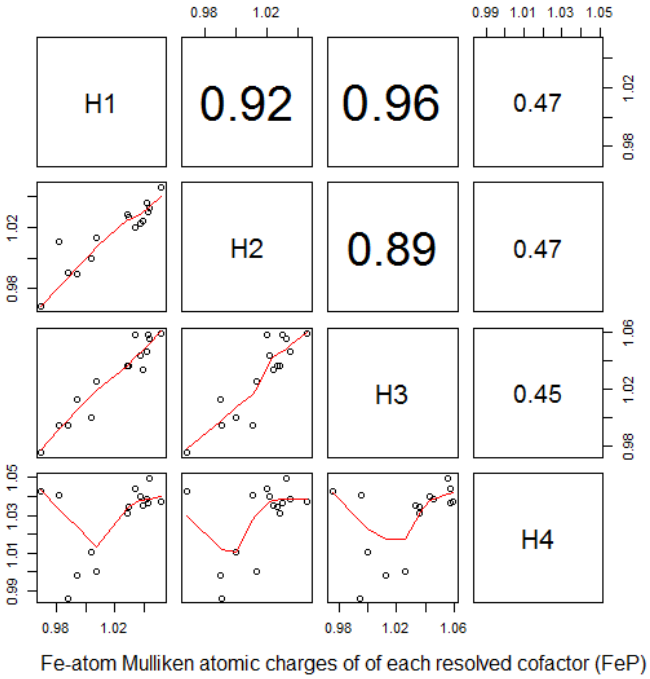

Figure 6: Scatter plot matrix of each PDB structures' vector of heme Fe-atom Mulliken charges obtained from B3LYP/3-21g wavefunctions of *Blastochloris viridis* RC cytochrome subunit heme macrocycle-only models (*i.e.* FeP-models [see experimental]) with the correlation coefficients (left). The correlation of cofactors H1-H3 indicates the propagation of the experimental systematic errors into the obtained Mulliken charges and highlights the need for an unbiased, critical method for data (conformation) selection such as we have performed.

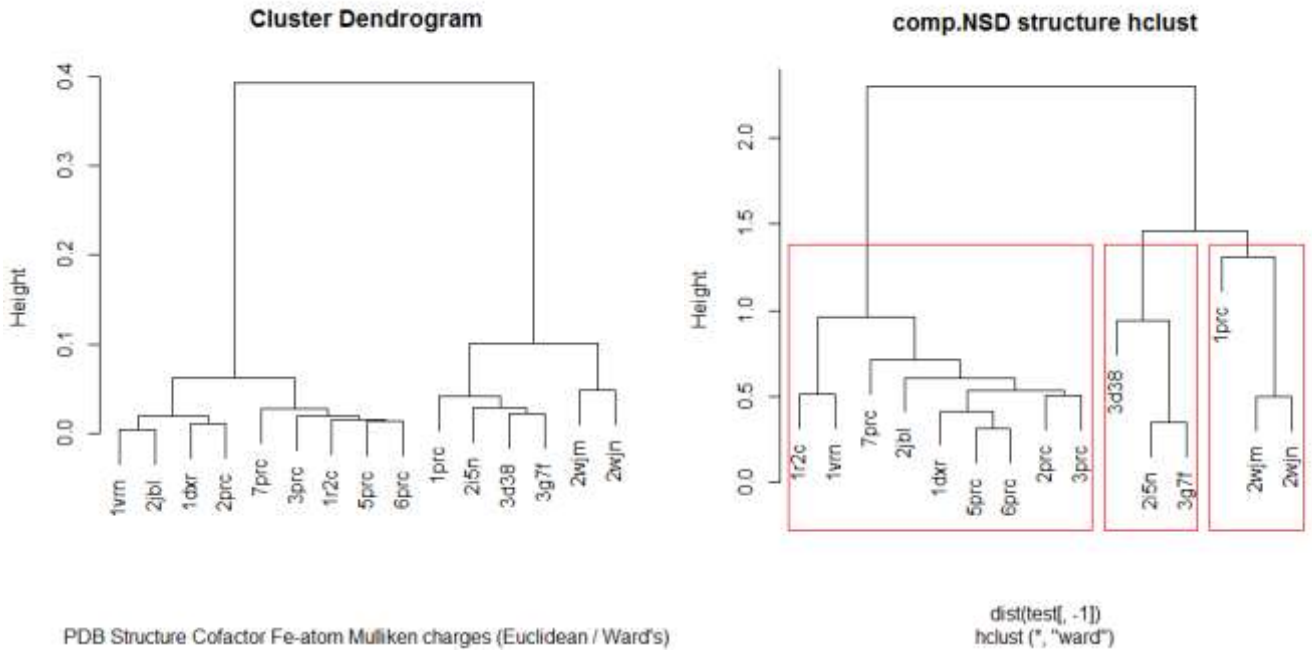

Figure 7: The cluster hierarchy of each PDB structures' vector of heme Fe-atom Mulliken charges obtained from B3LYP/3-21g wavefunctions of the four cofactors using the Euclidean metric and Ward's agglomeration (left) shown beside the dendrogram from the AHC of each structure's complete NSDs of the four cofactors (right). Considering a two cluster solution from the AHC of the Mulliken charges (left) and the corresponding two cluster solution from the conformational AHC (right; obtained by merging the two highlighted 3 structure clusters farthest to the right) yields identical cluster membership further indicating the dependance of the computed results on the bias of the structure selection.

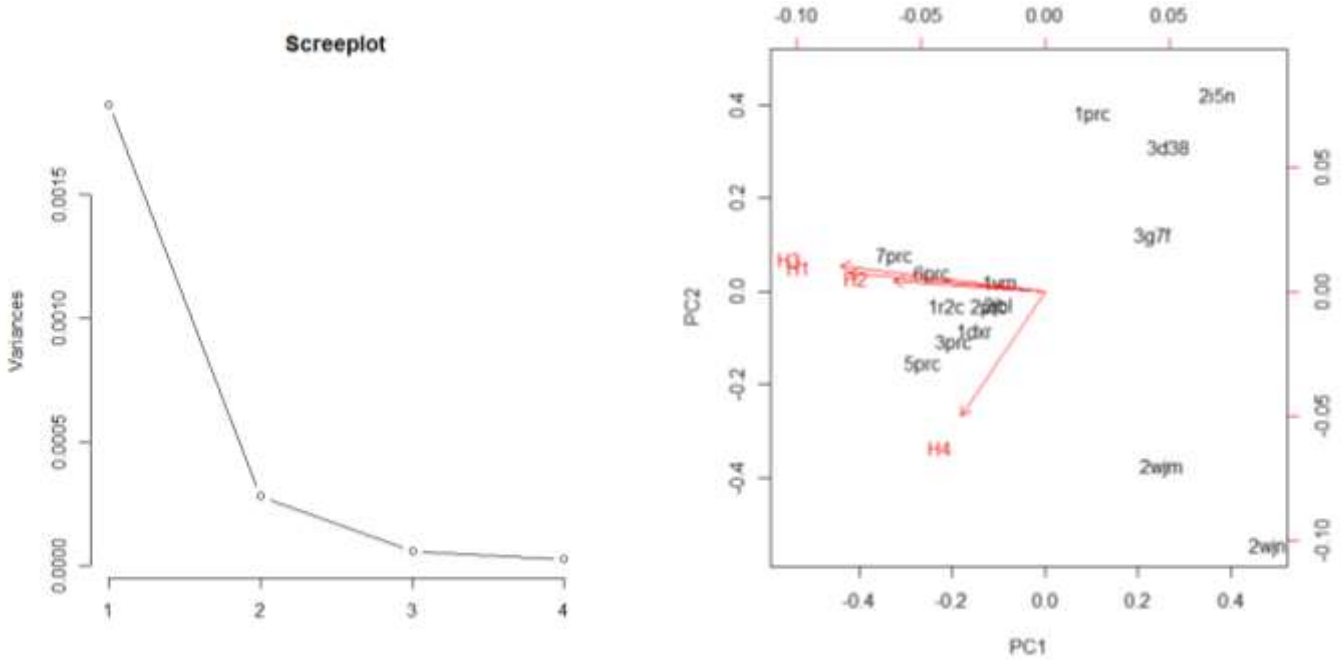

Figure 8: Scree-plot from the PCA of the Fe-atom Mulliken charges obtained from B3LYP/3-21g wavefunctions of each PDB structures' four cofactors (left) and the corresponding biplot (right).

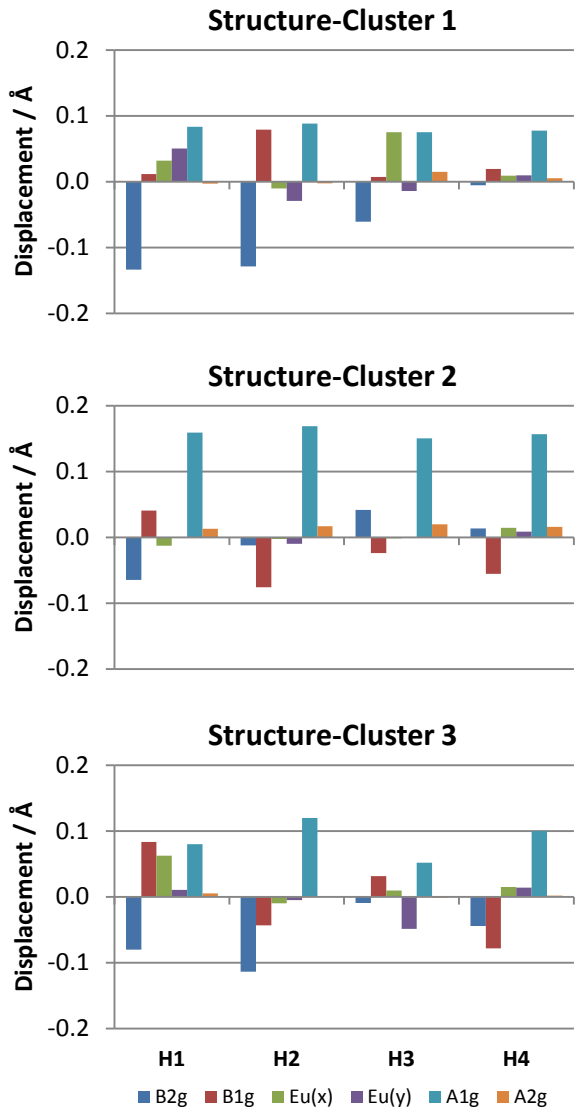

Figure 9: In-pane minimum basis NSDs for the structure-cluster mean conformations of the *B. viridis* hemes.

Data Section

Fe-Mulliken charges from individual cofactor coordinates

Table 2: Q_{Fe} derived from triplet state B3LYP/6-31g* single-point wavefunctions of H-NOx heme macrocycle-only models.

	Fe-atom Mulliken Atomic Charge / AU									
	Heme Diacid		FeP		FeP-comp		FeP-ext		FeP-min	
	Standard	*MBS*	*Standard*	*MBS*	*Standard*	*MBS*	*Standard*	*MBS*	*Standard*	*MBS*
1u56 - A500	1.085385	0.839044	1.089285	0.839754	1.086520	0.838624	0.913670	0.703113	1.088980	0.832352
1u56 - B501	0.924818	0.707208	1.064187	0.812055	1.063435	0.812383	1.084402	0.799069	1.085950	0.799522
3eee - A200	1.070607	0.746829	1.077064	0.751461	1.078335	0.750508	1.090139	0.782617	1.091643	0.784687
3eee - B200	1.074581	0.738786	1.076113	0.739825	1.076131	0.740093	1.090276	0.775031	1.066776	0.760865
3eee - C200	1.078828	0.746761	1.082851	0.749886	1.082608	0.749025	1.092905	0.774781	1.064978	0.757799
3eee - D200	1.081697	0.748437	1.082634	0.750568	1.081566	0.750627	1.092836	0.778848	1.064539	0.761230
3nvr - A200	1.079821	0.764057	1.078558	0.774116	1.077429	0.775527	1.064103	0.795681	1.066698	0.794930
3nvr - B200	1.077706	0.779062	1.081869	0.781892	1.081917	0.780243	1.089046	0.809821	1.064588	0.793071
3nvu - A200	1.074533	0.764057	1.078731	0.767173	1.078469	0.767564	1.066965	0.77863	1.068428	0.778375
3nvu - B200	1.081009	0.768753	1.084440	0.772172	1.085167	0.771793	1.091550	0.790059	1.091772	0.788684

Table 3: Q_{Fe} derived from triplet state B3LYP/6-311g single-point wavefunctions of H-NOx heme macrocycle-only models.**

	Fe-atom Mulliken Atomic Charge / AU									
	Heme Diacid		FeP		FeP-comp		FeP-ext		FeP-min	
	Standard	*MBS*	*Standard*	*MBS*	*Standard*	*MBS*	*Standard*	*MBS*	*Standard*	*MBS*
1u56 - A500	1.278694	0.663746	1.276234	0.667966	1.274895	0.667083	1.241882	0.641963	1.245335	0.642047
1u56 - B501	1.283163	0.651831	1.126432	0.560004	1.254255	0.645684	1.276867	0.636672	1.277996	0.636556
3eee - A200	1.279712	0.594615	1.280252	0.600893	1.280755	0.599440	1.284631	0.626345	1.287995	0.627157
3eee - B200	1.284858	0.590462	1.283206	0.593188	1.283408	0.593214	1.288020	0.621773	1.264039	0.609551
3eee - C200	1.289471	0.596064	1.289091	0.600903	1.289142	0.600025	1.291772	0.621673	1.262509	0.607214
3eee - D200	1.290516	0.598275	1.288433	0.600837	1.288092	0.601081	1.290984	0.624558	1.261411	0.609195
3nvr - A200	1.279254	0.614676	1.275996	0.616349	1.276031	0.617989	1.251697	0.634656	1.257292	0.633106
3nvr - B200	1.279641	0.617222	1.278837	0.622127	1.279039	0.620550	1.249527	0.631469	1.254959	0.630779
3nvu - A200	1.279618	0.605881	1.279152	0.610487	1.279378	0.611081	1.259107	0.621047	1.260885	0.621314
3nvu - B200	1.285935	0.610145	1.285178	0.614476	1.285197	0.613849	1.285270	0.630094	1.285493	0.629397

Table 4: Q_{Fe} derived from triplet state B3LYP/6-311+g single-point wavefunctions of H-NOx heme macrocycle-only models.**

	Fe-atom Mulliken Atomic Charge / AU									
	Heme Diacid		FeP		FeP-comp		FeP-ext		FeP-min	
	Standard	*MBS*	*Standard*	*MBS*	*Standard*	*MBS*	*Standard*	*MBS*	*Standard*	*MBS*
1u56 - A500			0.385919	0.558175	0.388961	0.557198	0.428268	0.534207	0.423738	0.535221
1u56 - B501			0.436471	0.540392	0.375785	0.532610	0.387412	0.522180	0.383853	0.521978
3eee - A200			0.440323	0.480272	0.439754	0.479172	0.431821	0.510805	0.433603	0.499813
3eee - B200			0.416277	0.470847	0.413914	0.471037	0.401254	0.504409	0.419452	0.496234
3eee - C200			0.419703	0.478653	0.421021	0.477917	0.405167	0.503768	0.401221	0.493491
3eee - D200			0.384463	0.479038	0.393366	0.479314	0.386034	0.507107	0.388617	0.502853
3nvr - A200			0.322924	0.498944	0.346901	0.500513	0.358456	0.525160	0.392923	0.522656
3nvr - B200			0.384849	0.504447	0.372952	0.503036	0.383796	0.522182	0.424258	0.521193
3nvu - A200			0.357646	0.490514	0.339600	0.491133	0.338054	0.505835	0.359959	0.506031
3nvu - B200			0.419772	0.494059	0.375591	0.493754	0.367439	0.513731	0.389717	0.513238

Table 5: Fe-atom Mulliken atomic charges derived from (R)B3LYP/3-21g single-point wavefunctions of *Blastochloris viridis* RC cytochrome subunit heme macrocycle-only models.

	Fe-atom Mulliken Charge		
Cofactor ID	No H-Opt/ rB3LYP 3-21g	PM6 H-Opt/ rB3LYP 3-21g	B3LYP H-Opt / rB3LYP 3-21g
1dxr - C401	1.037469	1.037018	1.036981
1dxr - C402	1.022490	1.021931	1.021925
1dxr - C403	1.043512	1.043126	1.043033
1dxr - C404	1.040821	1.040275	1.040149
1prc - C609	1.007409	1.007600	1.006995
1prc - C610	1.012567	1.013050	1.012347

	Fe-atom Mulliken Charge		
Cofactor ID	No H-Opt/ rB3LYP 3-21g	PM6 H-Opt/ rB3LYP 3-21g	B3LYP H-Opt / rB3LYP 3-21g
1prc - C611	1.025625	1.025697	1.025253
1prc - C612	1.000084	1.000132	0.999648
1r2c - C1201	1.034474	1.041103	1.041029
1r2c - C1202	1.036062	1.035567	1.035534
1r2c - C1203	1.046459	1.046058	1.045963
1r2c - C1204	1.039411	1.038940	1.038773
1vrn - C401	1.028533	1.028050	1.027964
1vrn - C402	1.029062	1.028529	1.028396
1VRN - C403	1.036501	1.036052	1.035951
1vrn - c404	1.031415	1.030967	1.030842
2i5n - c401	0.988849	0.988067	0.988122
2i5n - C402	0.991282	0.990579	0.990637
2i5n - C403	0.994890	0.994158	0.994204
2i5n - C404	0.986600	0.986042	0.986038
2jbl - c1333	1.029216	1.028864	1.028871
2jbl - C1334	1.027361	1.026780	1.026747
2jbl - C1335	1.036434	1.035995	1.035919
2jbl - C1336	1.034833	1.034418	1.034370
2prc - c337	1.038901	1.038545	1.038568
2prc - c338	1.024516	1.024118	1.024087
2prc - c339	1.033941	1.033521	1.033562
2prc - c340	1.035745	1.035324	1.035277
2wjm - c1333	0.982756	0.982360	0.982212
2WJM - C1334	1.011033	1.010755	1.010590
2wjm - c1335	0.995434	0.994796	0.994850
2wjm - c1336	1.041254	1.040906	1.040620
2wjn - c1333	0.970317	0.969867	0.969949
2wjn - c1334	0.968449	0.968051	0.968193
2wjn - c1335	0.975469	0.975143	0.975195
2wjn - c1336	1.043283	1.042985	1.042754
3d38 - C401	0.995015	0.994276	0.994534
3d38 - C402	0.990330	0.989865	0.989965
3d38 - C403	1.013118	1.012316	1.012449
3d38 - C404	0.998799	0.998264	0.998452
3g7f - C401	1.004172	1.003409	1.003382
3g7f - C402	1.000415	0.999792	0.999810
3g7f - C403	1.000495	0.999872	0.999929
3g7f - C404	1.011274	1.010730	1.010616
3prc - C337	1.034184	1.033786	1.033821
3prc - C338	1.020511	1.020163	1.020187
3PRC - C339	1.058238	1.057602	1.057468
3prc - C340	1.044931	1.044384	1.044225
5prc - C337	1.043181	1.042851	1.042810
5prc - C338	1.032650	1.032257	1.032193
5prc - C339	1.056355	1.055766	1.055680
5prc - C340	1.050020	1.049448	1.049299
6prc - C337	1.042500	1.042173	1.042213
6prc - C338	1.030408	1.029976	1.029901
6prc - C339	1.058546	1.058013	1.057845

	Fe-atom Mulliken Charge		
Cofactor ID	No H-Opt/ rB3LYP 3-21g	PM6 H-Opt/ rB3LYP 3-21g	B3LYP H-Opt / rB3LYP 3-21g
6prc - C340	1.037095	1.036579	1.036435
7prc - C337	1.051349	1.051189	1.051307
7prc - C338	1.046486	1.046037	1.045971
7prc - C339	1.059848	1.059372	1.059278
7PRC - C340	1.037511	1.037013	1.036933

Fe-Mulliken charges from mean cofactor coordinates

Table 6: Structure-cluster Fe-atom Mulliken atomic charges derived from triplet state B3LYP/6-31g* single-point wavefunctions of models of decreasing complexity of *Blastochloris viridis* RC cytochrome subunit hemes mean conformations.

		Fe-atom MBS Mulliken Atomic Charge / AU		
		FeP-comp	FeP-ext	FeP-min
Cluster 1	**H1**	0.749675	0.780551	0.779393
	H2	0.769364	0.778449	0.777697
	H3	0.769883	0.776665	0.776999
	H4	0.785283	0.793117	0.792090
Cluster 2	**H1**	0.754708	0.769294	0.768503
	H2	0.756958	0.764458	0.783147
	H3	0.758511	0.766292	0.783303
	H4	0.743767	0.765339	0.783342
Cluster 3	**H1**	0.777823	0.778036	0.777578
	H2	0.768664	0.773448	0.773414
	H3	0.800557	0.778363	0.778557
	H4	0.795073	0.773235	0.773408

Table 7: Structure-cluster Fe-atom Mulliken atomic charges derived from triplet state B3LYP/6-311g single-point wavefunctions of models of decreasing complexity of Blastochloris viridis RC cytochrome subunit hemes mean conformations.**

		Fe-atom MBS Mulliken Atomic Charge / AU		
		FeP-comp	FeP-ext	FeP-min
Cluster 1	**H1**	0.597240	0.622393	0.621734
	H2	0.613230	0.620288	0.620187
	H3	0.613341	0.619016	0.619051
	H4	0.624065	0.631995	0.631551
Cluster 2	**H1**	0.603668	0.614960	0.614430
	H2	0.603925	0.623862	0.611762
	H3	0.606320	0.612998	0.626304
	H4	0.606577	0.624121	0.626763
Cluster 3	**H1**	0.618971	0.619770	0.619711
	H2	0.613251	0.616962	0.617225
	H3	0.622627	0.619349	0.619910
	H4	0.630804	0.616605	0.616639

Table 8: Structure-cluster Fe-atom Mulliken atomic charges derived from triplet state B3LYP/6-311+g single-point wavefunctions of models of decreasing complexity of Blastochloris viridis RC cytochrome subunit hemes mean conformations.**

		Fe-atom MBS Mulliken Atomic Charge / AU		
		FeP-comp	FeP-ext	FeP-min
Cluster 1	**H1**	0.489164	0.510682	0.510089
	H2	0.494226	0.508560	0.508882
	H3	0.495363	0.507682	0.507544
	H4	0.505313	0.516045	0.505976
Cluster 2	**H1**	0.483297	0.501785	0.501441
	H2	0.483259	0.506703	0.498259
	H3	0.487204	0.501384	0.509845
	H4	0.486034	0.506812	0.499042
Cluster 3	**H1**	0.505269	0.508215	0.507704
	H2	0.499779	0.505106	0.505493
	H3	0.511380	0.508916	0.518505

	Fe-atom MBS Mulliken Atomic Charge / AU		
	FeP-comp	FeP-ext	FeP-min
H4	0.514082	0.504614	0.504587

DFT SCF Energies

Table 9: DFT SCF singlet and triplet energies of the FeP-comp. models of the H-NOx cofactors.

	DFT Singlet Energy / Hartrees	DFT Triplet Energy / Hartrees
1u56 - A500	-2240.632879	-2240.672832
1u56 - B501	-2240.636691	-2240.678924
3eee - A200	-2240.615036	-2240.681583
3eee - B200	-2240.613168	-2240.679820
3eee - C200	-2240.618125	-2240.683885
3eee - D200	-2240.615821	-2240.681473
3nvr - A200	-2240.607104	-2240.659521
3nvr - B200	-2240.616993	-2240.681487
3nvu - A200	-2240.606224	-2240.687748
3nvu - B200	-2240.629224	-2240.694401

Table 10: DFT SCF singlet and triplet energies of the FeP-ext. models of the H-NOx cofactors.

	DFT Singlet Energy / Hartrees	DFT Triplet Energy / Hartrees
1u56 - A500	-2240.637086	-
1u56 - B501	-2240.635064	-2240.714804
3eee - A200	-2240.645039	-2240.673961
3eee - B200	-2240.627234	-2240.670898
3eee - C200	-2240.646826	-2240.675277
3eee - D200	-2240.644858	-2240.682272
3nvr - A200	-2240.621035	-2240.701523
3nvr - B200	-2240.630456	-2240.671750
3nvu - A200	-2240.632483	-2240.713775
3nvu - B200	-2240.653694	-2240.681527

Table 11: DFT SCF singlet and triplet energies of the FeP-min. models of the H-NOx cofactors.

	DFT Singlet Energy / Hartrees	DFT Triplet Energy / Hartrees
1u56 - A500	-2240.636304	-2240.678368
1u56 - B501	-2240.635673	-2240.680695
3eee - A200	-2240.652073	-2240.681445
3eee - B200	-2240.633636	-2240.682090
3eee - C200	-2240.635279	-2240.678649
3eee - D200	-2240.634318	-2240.715800
3nvr - A200	-2240.632756	-2240.679974
3nvr - B200	-2240.640757	-2240.682348
3nvu - A200	-2240.635221	-2240.683447
3nvu - B200	-2240.655169	-2240.683767

Coordinates for Models of Reduced Complexity

Table 12: Coordinates for the non-H macrocycle atoms from the mean conformation of H1 from SC1.

	Minimum			Extended			Complete		
Atom	x	y	z	x	y	z	x	y	z
Fe	0.000	0.000	0.000	0.000	0.000	0.000	0.000	0.000	0.000
N1	-2.010	0.033	0.092	-2.010	0.035	0.026	-2.030	0.039	0.027
N2	-0.034	2.001	-0.052	-0.039	1.998	0.008	-0.038	2.029	0.012
N3	2.024	-0.030	0.036	2.029	-0.030	-0.006	2.057	-0.033	-0.009
N4	0.033	-2.024	-0.033	0.026	-2.022	0.008	0.033	-2.051	0.007

	Minimum			Extended			Complete		
Atom	x	y	z	x	y	z	x	y	z
Cm1	-2.446	2.446	0.080	-2.448	2.461	0.085	-2.438	2.452	0.086
Cm2	2.390	2.398	-0.098	2.391	2.402	-0.102	2.381	2.386	-0.104
Cm3	2.452	-2.448	0.047	2.447	-2.455	0.050	2.438	-2.444	0.050
Cm4	-2.400	-2.389	-0.027	-2.405	-2.399	-0.016	-2.396	-2.389	-0.013
Ca1	-2.829	-1.063	0.083	-2.830	-1.069	0.059	-2.834	-1.080	0.056
Ca2	-2.851	1.121	0.147	-2.848	1.131	0.114	-2.853	1.136	0.115
Ca3	-1.120	2.846	-0.044	-1.121	2.851	-0.011	-1.127	2.853	-0.019
Ca4	1.064	2.819	-0.160	1.061	2.813	-0.137	1.071	2.815	-0.138
Ca5	2.832	1.078	0.045	2.839	1.083	0.023	2.844	1.096	0.029
Ca6	2.870	-1.115	0.142	2.869	-1.121	0.126	2.867	-1.132	0.126
Ca7	1.120	-2.868	-0.084	1.115	-2.866	-0.068	1.128	-2.862	-0.064
Ca8	-1.077	-2.831	-0.105	-1.079	-2.834	-0.081	-1.089	-2.840	-0.083
Cb1	-4.212	-0.651	0.164	-4.210	-0.654	0.183	-4.200	-0.652	0.185
Cb2	-4.225	0.703	0.207	-4.219	0.703	0.222	-4.207	0.703	0.221
Cb3	-0.696	4.218	-0.189	-0.698	4.220	-0.204	-0.698	4.207	-0.199
Cb4	0.658	4.201	-0.266	0.654	4.194	-0.288	0.653	4.177	-0.290
Cb5	4.219	0.687	0.227	4.225	0.689	0.237	4.212	0.717	0.235
Cb6	4.244	-0.670	0.295	4.243	-0.671	0.312	4.224	-0.695	0.313
Cb7	0.676	-4.242	-0.249	0.682	-4.240	-0.270	0.678	-4.222	-0.273
Cb8	-0.682	-4.218	-0.259	-0.674	-4.218	-0.270	-0.674	-4.209	-0.267

Table 13: Coordinates for the non-H macrocycle atoms from the mean conformation of H2 from SC1.

	Minimum			Extended			Complete		
Atom	x	y	z	x	y	z	x	y	z
Fe	0.000	0.000	0.000	0.000	0.000	0.000	0.000	0.000	0.000
N1	-2.033	0.030	0.045	-2.040	0.033	0.014	-2.063	0.031	0.018
N2	-0.032	2.007	-0.050	-0.025	2.003	-0.013	-0.027	2.027	-0.010
N3	2.029	-0.031	0.009	2.030	-0.032	-0.027	2.063	-0.043	-0.030
N4	0.032	-1.994	-0.026	0.039	-1.990	-0.005	0.049	-2.002	-0.008
Cm1	-2.456	2.441	0.139	-2.454	2.455	0.141	-2.449	2.443	0.143
Cm2	2.404	2.388	-0.162	2.411	2.403	-0.160	2.406	2.395	-0.154
Cm3	2.452	-2.441	0.127	2.454	-2.462	0.136	2.443	-2.452	0.135
Cm4	-2.399	-2.391	-0.105	-2.398	-2.399	-0.100	-2.391	-2.385	-0.106
Ca1	-2.846	-1.074	-0.004	-2.849	-1.082	-0.012	-2.848	-1.087	-0.017
Ca2	-2.879	1.114	0.138	-2.883	1.124	0.121	-2.880	1.127	0.119
Ca3	-1.122	2.849	0.024	-1.115	2.848	0.042	-1.127	2.853	0.034
Ca4	1.076	2.817	-0.159	1.080	2.816	-0.142	1.090	2.825	-0.144
Ca5	2.847	1.067	-0.038	2.847	1.078	-0.054	2.848	1.090	-0.051
Ca6	2.871	-1.119	0.144	2.869	-1.130	0.131	2.863	-1.140	0.131
Ca7	1.120	-2.837	0.003	1.120	-2.846	0.015	1.127	-2.844	0.023
Ca8	-1.070	-2.808	-0.119	-1.067	-2.799	-0.110	-1.078	-2.809	-0.109
Cb1	-4.234	-0.680	0.073	-4.235	-0.693	0.084	-4.225	-0.692	0.092
Cb2	-4.255	0.677	0.168	-4.257	0.668	0.173	-4.249	0.670	0.168
Cb3	-0.683	4.221	-0.060	-0.680	4.218	-0.074	-0.677	4.203	-0.065
Cb4	0.674	4.200	-0.181	0.674	4.196	-0.191	0.675	4.178	-0.199
Cb5	4.233	0.659	0.108	4.228	0.671	0.115	4.220	0.701	0.107
Cb6	4.248	-0.696	0.231	4.241	-0.688	0.243	4.220	-0.712	0.248

	Minimum			Extended			Complete		
Atom	x	y	z	x	y	z	x	y	z
Cb7	0.689	-4.208	-0.113	0.681	-4.212	-0.125	0.681	-4.201	-0.134
Cb8	-0.666	-4.190	-0.192	-0.671	-4.179	-0.200	-0.671	-4.175	-0.192

Table 14: Coordinates for the non-H macrocycle atoms from the mean conformation of H3 from SC1.

	Minimum			Extended			Complete		
Atom	x	y	z	x	y	z	x	y	z
Fe	0.000	0.000	0.000	0.000	0.000	0.000	0.000	0.000	0.000
N1	-1.997	0.019	0.034	-1.999	0.014	-0.016	-2.023	0.021	-0.013
N2	-0.012	2.015	-0.007	-0.016	2.016	0.025	-0.015	2.034	0.021
N3	2.031	-0.019	0.014	2.037	-0.030	-0.017	2.057	-0.028	-0.025
N4	0.009	-2.008	-0.071	0.002	-2.003	-0.033	0.002	-2.022	-0.028
Cm1	-2.436	2.426	0.233	-2.425	2.435	0.243	-2.414	2.426	0.239
Cm2	2.408	2.412	-0.174	2.400	2.404	-0.171	2.394	2.395	-0.170
Cm3	2.428	-2.439	0.154	2.421	-2.449	0.155	2.422	-2.438	0.159
Cm4	-2.411	-2.401	-0.214	-2.417	-2.406	-0.207	-2.406	-2.394	-0.211
Ca1	-2.820	-1.077	-0.078	-2.828	-1.085	-0.099	-2.835	-1.091	-0.097
Ca2	-2.841	1.101	0.201	-2.831	1.104	0.180	-2.825	1.111	0.174
Ca3	-1.112	2.841	0.075	-1.106	2.855	0.096	-1.111	2.865	0.103
Ca4	1.079	2.844	-0.173	1.073	2.836	-0.162	1.081	2.831	-0.160
Ca5	2.848	1.085	-0.032	2.849	1.082	-0.043	2.845	1.097	-0.039
Ca6	2.865	-1.114	0.139	2.869	-1.123	0.124	2.866	-1.130	0.134
Ca7	1.095	-2.848	0.033	1.086	-2.849	0.049	1.100	-2.847	0.040
Ca8	-1.092	-2.827	-0.181	-1.095	-2.822	-0.159	-1.107	-2.828	-0.162
Cb1	-4.199	-0.679	0.035	-4.206	-0.690	0.045	-4.202	-0.687	0.043
Cb2	-4.214	0.673	0.222	-4.205	0.665	0.235	-4.190	0.653	0.240
Cb3	-0.710	4.220	-0.089	-0.708	4.234	-0.100	-0.705	4.222	-0.098
Cb4	0.647	4.224	-0.257	0.646	4.219	-0.271	0.639	4.208	-0.276
Cb5	4.232	0.672	0.101	4.236	0.690	0.110	4.223	0.713	0.110
Cb6	4.244	-0.686	0.211	4.248	-0.671	0.219	4.243	-0.703	0.213
Cb7	0.657	-4.223	-0.015	0.660	-4.223	-0.034	0.650	-4.208	-0.036
Cb8	-0.698	-4.209	-0.158	-0.693	-4.202	-0.167	-0.689	-4.200	-0.162

Table 15: Coordinates for the non-H macrocycle atoms from the mean conformation of H4 from SC1.

	Minimum			Extended			Complete		
Atom	x	y	z	x	y	z	x	y	z
Fe	0.000	0.000	0.000	0.000	0.000	0.000	0.000	0.000	0.000
N1	-2.015	0.003	0.022	-2.022	0.004	0.014	-2.032	0.007	0.017
N2	0.000	2.008	0.005	0.003	2.002	0.006	-0.002	2.005	0.001
N3	2.019	-0.003	0.018	2.024	-0.003	0.004	2.044	0.001	0.001
N4	0.000	-2.012	-0.031	0.002	-2.006	-0.027	0.003	-2.009	-0.030
Cm1	-2.422	2.420	0.080	-2.417	2.433	0.088	-2.407	2.421	0.078
Cm2	2.420	2.419	-0.046	2.418	2.434	-0.037	2.410	2.424	-0.038
Cm3	2.423	-2.421	0.043	2.420	-2.437	0.050	2.417	-2.431	0.054
Cm4	-2.422	-2.416	-0.076	-2.418	-2.428	-0.069	-2.420	-2.414	-0.070
Ca1	-2.844	-1.091	-0.013	-2.846	-1.101	-0.014	-2.844	-1.106	-0.015
Ca2	-2.845	1.096	0.080	-2.847	1.107	0.078	-2.844	1.110	0.077

	Minimum			Extended			Complete		
Atom	x	y	z	x	y	z	x	y	z
Ca3	-1.096	2.836	0.019	-1.089	2.833	0.022	-1.099	2.839	0.033
Ca4	1.093	2.837	-0.066	1.090	2.837	-0.064	1.100	2.844	-0.060
Ca5	2.845	1.094	0.016	2.846	1.105	0.014	2.839	1.122	0.013
Ca6	2.850	-1.095	0.048	2.849	-1.107	0.042	2.845	-1.119	0.047
Ca7	1.095	-2.840	0.001	1.091	-2.842	0.008	1.101	-2.850	0.011
Ca8	-1.096	-2.839	-0.077	-1.090	-2.835	-0.075	-1.105	-2.836	-0.072
Cb1	-4.223	-0.675	0.037	-4.224	-0.679	0.034	-4.218	-0.675	0.030
Cb2	-4.224	0.681	0.097	-4.224	0.681	0.098	-4.223	0.674	0.106
Cb3	-0.682	4.214	-0.070	-0.681	4.210	-0.075	-0.680	4.201	-0.074
Cb4	0.673	4.215	-0.130	0.670	4.213	-0.132	0.677	4.209	-0.137
Cb5	4.226	0.682	0.064	4.224	0.685	0.064	4.216	0.719	0.070
Cb6	4.229	-0.674	0.081	4.226	-0.675	0.083	4.221	-0.713	0.074
Cb7	0.676	-4.219	-0.023	0.673	-4.218	-0.028	0.675	-4.214	-0.034
Cb8	-0.680	-4.218	-0.079	-0.680	-4.213	-0.084	-0.672	-4.210	-0.080

Table 16: Coordinates for the non-H macrocycle atoms from the mean conformation of H1 from SC2.

	Minimum			Extended			Complete		
Atom	x	y	z	x	y	z	x	y	z
Fe	0.000	0.000	0.000	0.000	0.000	0.000	0.000	0.000	0.000
N1	-2.041	0.019	0.043	-2.042	0.013	-0.028	-2.067	0.014	-0.034
N2	-0.012	2.022	-0.141	-0.009	2.025	-0.064	-0.010	2.039	-0.065
N3	2.035	-0.019	-0.001	2.034	-0.030	-0.090	2.074	-0.034	-0.100
N4	0.012	-2.022	-0.039	0.016	-2.019	0.081	0.014	-2.049	0.087
Cm1	-2.443	2.440	0.067	-2.442	2.445	0.067	-2.434	2.432	0.060
Cm2	2.419	2.410	-0.166	2.424	2.413	-0.184	2.413	2.397	-0.208
Cm3	2.444	-2.438	0.122	2.455	-2.454	0.112	2.445	-2.444	0.119
Cm4	-2.418	-2.412	-0.030	-2.430	-2.419	-0.070	-2.421	-2.409	-0.055
Ca1	-2.859	-1.086	0.086	-2.867	-1.093	0.043	-2.864	-1.105	0.041
Ca2	-2.878	1.113	0.121	-2.874	1.112	0.090	-2.872	1.122	0.101
Ca3	-1.109	2.856	-0.063	-1.107	2.861	-0.038	-1.118	2.857	-0.040
Ca4	1.092	2.843	-0.206	1.097	2.844	-0.169	1.110	2.843	-0.158
Ca5	2.855	1.084	-0.016	2.849	1.084	-0.051	2.854	1.101	-0.025
Ca6	2.874	-1.111	0.190	2.879	-1.120	0.135	2.876	-1.133	0.135
Ca7	1.111	-2.854	-0.060	1.116	-2.859	-0.011	1.132	-2.860	-0.020
Ca8	-1.089	-2.845	-0.130	-1.094	-2.835	-0.083	-1.109	-2.836	-0.093
Cb1	-4.246	-0.677	0.228	-4.250	-0.685	0.264	-4.239	-0.673	0.254
Cb2	-4.259	0.682	0.249	-4.253	0.674	0.276	-4.247	0.665	0.281
Cb3	-0.680	4.234	-0.097	-0.677	4.239	-0.131	-0.668	4.236	-0.132
Cb4	0.678	4.227	-0.191	0.681	4.226	-0.196	0.675	4.226	-0.193
Cb5	4.240	0.676	0.226	4.233	0.692	0.279	4.216	0.689	0.280
Cb6	4.254	-0.681	0.370	4.254	-0.666	0.385	4.231	-0.661	0.378
Cb7	0.689	-4.233	-0.261	0.683	-4.232	-0.295	0.677	-4.217	-0.289
Cb8	-0.669	-4.228	-0.302	-0.675	-4.215	-0.320	-0.667	-4.198	-0.324

Table 17: Coordinates for the non-H macrocycle atoms from the mean conformation of H2 from SC2.

	Minimum			Extended			Complete		

Atom	x	y	z	x	y	z	x	y	z
Fe	0.000	0.000	0.000	0.000	0.000	0.000	0.000	0.000	0.000
N1	-2.018	0.008	0.003	-2.018	0.003	-0.050	-2.041	0.007	-0.054
N2	0.002	2.049	-0.124	0.004	2.051	-0.082	0.000	2.065	-0.079
N3	2.016	-0.008	-0.004	2.016	-0.014	-0.055	2.033	-0.019	-0.064
N4	-0.002	-2.044	-0.013	-0.002	-2.042	0.086	0.000	-2.069	0.091
Cm1	-2.426	2.438	0.096	-2.426	2.444	0.101	-2.417	2.431	0.089
Cm2	2.422	2.431	-0.203	2.428	2.433	-0.223	2.414	2.421	-0.242
Cm3	2.424	-2.438	0.193	2.431	-2.450	0.178	2.416	-2.441	0.199
Cm4	-2.421	-2.432	-0.093	-2.432	-2.438	-0.132	-2.428	-2.428	-0.125
Ca1	-2.840	-1.098	0.022	-2.847	-1.103	-0.019	-2.849	-1.116	-0.018
Ca2	-2.850	1.105	0.091	-2.844	1.107	0.074	-2.842	1.119	0.085
Ca3	-1.098	2.876	-0.002	-1.099	2.880	0.009	-1.115	2.871	0.000
Ca4	1.099	2.879	-0.190	1.102	2.879	-0.169	1.115	2.876	-0.158
Ca5	2.840	1.096	-0.074	2.839	1.095	-0.092	2.841	1.115	-0.064
Ca6	2.847	-1.107	0.182	2.848	-1.115	0.143	2.843	-1.131	0.133
Ca7	1.098	-2.872	0.035	1.101	-2.874	0.067	1.119	-2.874	0.052
Ca8	-1.097	-2.876	-0.142	-1.102	-2.871	-0.097	-1.118	-2.866	-0.103
Cb1	-4.221	-0.684	0.153	-4.225	-0.683	0.183	-4.209	-0.677	0.172
Cb2	-4.229	0.674	0.191	-4.222	0.675	0.209	-4.212	0.668	0.218
Cb3	-0.681	4.261	0.018	-0.686	4.263	0.000	-0.675	4.256	0.014
Cb4	0.677	4.264	-0.111	0.673	4.263	-0.113	0.670	4.270	-0.122
Cb5	4.221	0.677	0.096	4.218	0.681	0.145	4.217	0.683	0.143
Cb6	4.227	-0.681	0.267	4.224	-0.677	0.266	4.216	-0.677	0.262
Cb7	0.683	-4.257	-0.136	0.687	-4.254	-0.163	0.683	-4.244	-0.166
Cb8	-0.675	-4.260	-0.256	-0.671	-4.253	-0.266	-0.661	-4.240	-0.262

Table 18: Coordinates for the non-H macrocycle atoms from the mean conformation of H3 from SC2.

	Minimum			Extended			Complete		
Atom	x	y	z	x	y	z	x	y	z
Fe	0.000	0.000	0.000	0.000	0.000	0.000	0.000	0.000	0.000
N1	-2.024	-0.005	-0.051	-2.027	0.002	-0.085	-2.056	0.005	-0.093
N2	0.016	2.033	-0.108	0.019	2.031	-0.069	0.018	2.045	-0.068
N3	2.023	0.005	0.014	2.023	0.007	0.002	2.041	0.004	-0.003
N4	-0.016	-2.033	-0.060	-0.012	-2.034	0.004	-0.016	-2.055	0.006
Cm1	-2.416	2.422	0.158	-2.412	2.423	0.162	-2.407	2.411	0.150
Cm2	2.435	2.436	-0.208	2.437	2.437	-0.258	2.425	2.430	-0.264
Cm3	2.416	-2.422	0.264	2.410	-2.424	0.252	2.399	-2.415	0.270
Cm4	-2.435	-2.437	-0.224	-2.428	-2.429	-0.275	-2.419	-2.417	-0.285
Ca1	-2.853	-1.104	-0.068	-2.853	-1.101	-0.094	-2.856	-1.115	-0.086
Ca2	-2.850	1.095	0.138	-2.855	1.096	0.118	-2.850	1.109	0.134
Ca3	-1.088	2.853	0.015	-1.082	2.854	0.022	-1.100	2.845	0.019
Ca4	1.109	2.869	-0.187	1.111	2.867	-0.173	1.125	2.864	-0.168
Ca5	2.853	1.104	-0.083	2.855	1.107	-0.091	2.855	1.122	-0.070
Ca6	2.850	-1.094	0.204	2.846	-1.093	0.183	2.843	-1.106	0.168
Ca7	1.088	-2.853	0.089	1.085	-2.862	0.097	1.100	-2.859	0.084
Ca8	-1.108	-2.870	-0.223	-1.105	-2.865	-0.191	-1.119	-2.857	-0.182
Cb1	-4.233	-0.684	0.161	-4.235	-0.696	0.204	-4.220	-0.691	0.202
Cb2	-4.232	0.674	0.294	-4.238	0.662	0.293	-4.224	0.656	0.291
Cb3	-0.678	4.238	-0.001	-0.675	4.239	-0.019	-0.666	4.234	-0.007

	Minimum			Extended			Complete		
Atom	x	y	z	x	y	z	x	y	z
Cb4	0.680	4.250	-0.135	0.682	4.247	-0.120	0.681	4.249	-0.131
Cb5	4.232	0.684	0.044	4.235	0.693	0.092	4.229	0.686	0.081
Cb6	4.232	-0.674	0.235	4.229	-0.665	0.222	4.224	-0.659	0.228
Cb7	0.679	-4.238	-0.027	0.673	-4.248	-0.056	0.665	-4.246	-0.060
Cb8	-0.679	-4.250	-0.239	-0.684	-4.248	-0.221	-0.672	-4.240	-0.218

Table 19: Coordinates for the non-H macrocycle atoms from the mean conformation of H4 from SC2.

	Minimum			Extended			Complete		
Atom	x	y	z	x	y	z	x	y	z
Fe	0.000	0.000	0.000	0.000	0.000	0.000	0.000	0.000	0.000
N1	-2.015	0.001	-0.026	-2.019	-0.001	-0.030	-2.033	0.002	-0.031
N2	0.007	2.038	-0.094	0.015	2.038	-0.053	0.010	2.054	-0.052
N3	2.022	-0.001	-0.050	2.019	-0.003	-0.077	2.041	-0.010	-0.087
N4	-0.008	-2.042	-0.060	-0.001	-2.041	-0.012	0.001	-2.057	-0.014
Cm1	-2.420	2.429	0.103	-2.420	2.431	0.082	-2.411	2.417	0.078
Cm2	2.426	2.436	-0.140	2.434	2.445	-0.171	2.425	2.437	-0.184
Cm3	2.420	-2.431	0.111	2.430	-2.443	0.096	2.419	-2.436	0.101
Cm4	-2.428	-2.433	-0.085	-2.432	-2.435	-0.127	-2.424	-2.426	-0.128
Ca1	-2.843	-1.099	-0.022	-2.849	-1.101	-0.035	-2.846	-1.117	-0.032
Ca2	-2.844	1.100	0.074	-2.844	1.102	0.065	-2.839	1.116	0.067
Ca3	-1.094	2.862	0.018	-1.093	2.857	0.020	-1.110	2.852	0.012
Ca4	1.100	2.873	-0.137	1.106	2.879	-0.118	1.121	2.875	-0.107
Ca5	2.847	1.103	-0.060	2.844	1.106	-0.079	2.848	1.121	-0.058
Ca6	2.850	-1.100	0.092	2.849	-1.107	0.072	2.843	-1.122	0.074
Ca7	1.092	-2.868	0.010	1.100	-2.872	0.024	1.114	-2.867	0.026
Ca8	-1.104	-2.874	-0.103	-1.103	-2.868	-0.090	-1.119	-2.864	-0.088
Cb1	-4.223	-0.678	0.084	-4.227	-0.676	0.110	-4.222	-0.672	0.103
Cb2	-4.224	0.679	0.144	-4.224	0.682	0.150	-4.221	0.679	0.155
Cb3	-0.685	4.247	0.037	-0.691	4.241	0.026	-0.685	4.232	0.037
Cb4	0.673	4.255	-0.069	0.666	4.258	-0.059	0.665	4.261	-0.068
Cb5	4.228	0.685	0.097	4.221	0.684	0.129	4.216	0.682	0.126
Cb6	4.231	-0.673	0.198	4.225	-0.675	0.204	4.212	-0.668	0.200
Cb7	0.675	-4.252	-0.023	0.675	-4.253	-0.028	0.670	-4.246	-0.034
Cb8	-0.683	-4.257	-0.099	-0.683	-4.250	-0.098	-0.676	-4.247	-0.095

Table 20: Coordinates for the non-H macrocycle atoms from the mean conformation of H1 from SC3.

	Minimum			Extended			Complete		
Atom	x	y	z	x	y	z	x	y	z
Fe	0.000	0.000	0.000	0.000	0.000	0.000	0.000	0.000	0.000
N1	-2.016	0.021	0.074	-2.013	0.024	0.004	-2.019	0.032	0.012
N2	-0.019	1.996	-0.019	-0.022	1.995	0.001	-0.024	1.999	-0.008
N3	2.044	-0.021	0.002	2.044	-0.017	0.032	2.042	-0.017	0.044
N4	0.017	-2.000	-0.037	0.012	-2.003	-0.036	0.015	-1.998	-0.053
Cm1	-2.444	2.426	0.147	-2.450	2.430	0.152	-2.444	2.422	0.132
Cm2	2.408	2.403	-0.130	2.414	2.402	-0.125	2.414	2.400	-0.122
Cm3	2.442	-2.435	0.063	2.440	-2.432	0.039	2.443	-2.430	0.064

	Minimum			Extended			Complete		
Atom	x	y	z	x	y	z	x	y	z
Cm4	-2.414	-2.392	-0.079	-2.419	-2.392	-0.032	-2.417	-2.393	-0.045
Ca1	-2.840	-1.072	-0.014	-2.839	-1.069	-0.029	-2.842	-1.074	-0.020
Ca2	-2.858	1.105	0.170	-2.857	1.108	0.132	-2.861	1.114	0.121
Ca3	-1.116	2.827	0.011	-1.121	2.828	0.057	-1.122	2.831	0.055
Ca4	1.076	2.820	-0.127	1.077	2.817	-0.151	1.079	2.818	-0.122
Ca5	2.860	1.083	-0.027	2.866	1.082	-0.009	2.867	1.084	-0.028
Ca6	2.882	-1.111	0.128	2.877	-1.109	0.136	2.879	-1.112	0.118
Ca7	1.105	-2.840	-0.057	1.105	-2.839	-0.057	1.109	-2.838	-0.037
Ca8	-1.090	-2.814	-0.073	-1.093	-2.818	-0.065	-1.097	-2.821	-0.058
Cb1	-4.223	-0.669	0.020	-4.221	-0.665	0.005	-4.220	-0.650	-0.013
Cb2	-4.235	0.685	0.162	-4.231	0.687	0.197	-4.224	0.671	0.223
Cb3	-0.705	4.201	-0.121	-0.712	4.200	-0.107	-0.704	4.200	-0.071
Cb4	0.650	4.198	-0.198	0.644	4.194	-0.230	0.633	4.189	-0.270
Cb5	4.247	0.678	0.129	4.253	0.672	0.092	4.256	0.668	0.111
Cb6	4.262	-0.680	0.248	4.258	-0.686	0.276	4.252	-0.681	0.262
Cb7	0.662	-4.213	-0.140	0.672	-4.212	-0.156	0.663	-4.209	-0.195
Cb8	-0.694	-4.195	-0.131	-0.685	-4.198	-0.126	-0.681	-4.205	-0.099

Table 21: Coordinates for the non-H macrocycle atoms from the mean conformation of H2 from SC3.

	Minimum			Extended			Complete		
Atom	x	y	z	x	y	z	x	y	z
Fe	0.000	0.000	0.000	0.000	0.000	0.000	0.000	0.000	0.000
N1	-2.016	0.028	0.033	-2.018	0.030	-0.021	-2.018	0.035	-0.027
N2	-0.027	2.031	-0.074	-0.022	2.030	-0.080	-0.031	2.035	-0.094
N3	2.011	-0.028	-0.009	2.011	-0.027	-0.022	2.015	-0.035	0.001
N4	0.028	-2.029	-0.033	0.029	-2.029	-0.015	0.034	-2.038	-0.034
Cm1	-2.444	2.451	0.178	-2.438	2.456	0.195	-2.432	2.451	0.206
Cm2	2.399	2.404	-0.218	2.404	2.406	-0.176	2.405	2.410	-0.184
Cm3	2.444	-2.450	0.177	2.439	-2.457	0.172	2.432	-2.455	0.157
Cm4	-2.397	-2.406	-0.141	-2.397	-2.402	-0.093	-2.398	-2.402	-0.097
Ca1	-2.829	-1.078	-0.023	-2.835	-1.076	-0.051	-2.837	-1.078	-0.052
Ca2	-2.857	1.119	0.152	-2.854	1.123	0.148	-2.854	1.122	0.156
Ca3	-1.116	2.874	0.048	-1.112	2.874	0.061	-1.113	2.874	0.071
Ca4	1.077	2.847	-0.199	1.078	2.846	-0.201	1.078	2.852	-0.184
Ca5	2.827	1.076	-0.074	2.833	1.077	-0.077	2.837	1.076	-0.085
Ca6	2.853	-1.119	0.170	2.845	-1.123	0.174	2.849	-1.124	0.144
Ca7	1.117	-2.871	0.028	1.116	-2.876	0.035	1.118	-2.881	0.056
Ca8	-1.074	-2.846	-0.148	-1.071	-2.842	-0.125	-1.075	-2.847	-0.100
Cb1	-4.214	-0.673	0.073	-4.220	-0.674	0.056	-4.218	-0.669	0.069
Cb2	-4.231	0.684	0.187	-4.229	0.684	0.210	-4.232	0.682	0.191
Cb3	-0.682	4.251	-0.015	-0.694	4.251	0.004	-0.683	4.245	-0.017
Cb4	0.675	4.233	-0.181	0.662	4.232	-0.222	0.654	4.229	-0.212
Cb5	4.211	0.669	0.105	4.215	0.669	0.089	4.216	0.661	0.078
Cb6	4.227	-0.687	0.268	4.219	-0.689	0.276	4.210	-0.678	0.304
Cb7	0.689	-4.248	-0.095	0.698	-4.253	-0.093	0.691	-4.244	-0.081
Cb8	-0.668	-4.233	-0.211	-0.658	-4.229	-0.243	-0.649	-4.221	-0.267

Table 22: Coordinates for the non-H macrocycle atoms from the mean conformation of H3 from SC3.

	Minimum			Extended			Complete		
Atom	x	y	z	x	y	z	x	y	z
Fe	0.000	0.000	0.000	0.000	0.000	0.000	0.000	0.000	0.000
N1	-2.012	0.001	0.036	-2.016	0.001	-0.031	-2.010	0.005	-0.030
N2	-0.003	2.013	-0.021	0.005	2.012	-0.058	-0.003	2.012	-0.078
N3	2.016	-0.003	0.002	2.015	-0.004	0.026	2.008	-0.008	0.037
N4	0.002	-1.991	-0.062	0.008	-1.990	-0.040	0.010	-1.989	-0.049
Cm1	-2.427	2.415	0.205	-2.419	2.415	0.239	-2.410	2.412	0.229
Cm2	2.422	2.413	-0.168	2.425	2.415	-0.130	2.429	2.422	-0.133
Cm3	2.418	-2.420	0.135	2.416	-2.428	0.116	2.415	-2.424	0.121
Cm4	-2.415	-2.415	-0.174	-2.413	-2.410	-0.125	-2.413	-2.407	-0.133
Ca1	-2.837	-1.095	-0.056	-2.844	-1.094	-0.092	-2.846	-1.094	-0.086
Ca2	-2.847	1.088	0.177	-2.845	1.090	0.174	-2.843	1.089	0.172
Ca3	-1.100	2.839	0.063	-1.094	2.837	0.075	-1.092	2.841	0.092
Ca4	1.094	2.838	-0.168	1.097	2.840	-0.194	1.097	2.842	-0.166
Ca5	2.848	1.086	-0.034	2.849	1.087	-0.012	2.848	1.091	-0.024
Ca6	2.842	-1.099	0.130	2.837	-1.104	0.140	2.840	-1.109	0.127
Ca7	1.091	-2.824	0.019	1.092	-2.831	0.019	1.099	-2.831	0.030
Ca8	-1.089	-2.820	-0.155	-1.085	-2.813	-0.123	-1.091	-2.818	-0.114
Cb1	-4.217	-0.693	0.040	-4.224	-0.695	0.017	-4.227	-0.690	0.013
Cb2	-4.224	0.661	0.195	-4.224	0.660	0.223	-4.229	0.652	0.228
Cb3	-0.682	4.218	-0.072	-0.691	4.217	-0.042	-0.678	4.219	-0.038
Cb4	0.675	4.217	-0.228	0.665	4.219	-0.267	0.651	4.212	-0.284
Cb5	4.227	0.660	0.110	4.227	0.662	0.093	4.229	0.659	0.098
Cb6	4.222	-0.695	0.217	4.216	-0.694	0.211	4.217	-0.695	0.213
Cb7	0.674	-4.199	-0.037	0.677	-4.205	-0.047	0.670	-4.201	-0.058
Cb8	-0.679	-4.196	-0.152	-0.675	-4.190	-0.171	-0.670	-4.191	-0.166

Table 23: Coordinates for the non-H macrocycle atoms from the mean conformation of H4 from SC3.

	Minimum			Extended			Complete		
Atom	x	y	z	x	y	z	x	y	z
Fe	0.000	0.000	0.000	0.000	0.000	0.000	0.000	0.000	0.000
N1	-1.999	0.012	0.034	-2.001	0.013	0.021	-1.995	0.019	0.017
N2	-0.011	2.030	0.029	-0.006	2.029	0.013	-0.010	2.028	-0.002
N3	2.006	-0.011	0.025	2.005	-0.009	0.032	2.006	-0.010	0.032
N4	0.010	-2.036	-0.033	0.011	-2.037	-0.072	0.015	-2.030	-0.074
Cm1	-2.425	2.437	0.138	-2.420	2.435	0.155	-2.409	2.428	0.148
Cm2	2.406	2.421	-0.078	2.408	2.422	-0.047	2.411	2.420	-0.059
Cm3	2.426	-2.438	0.071	2.422	-2.439	0.090	2.424	-2.438	0.088
Cm4	-2.409	-2.418	-0.128	-2.407	-2.413	-0.083	-2.409	-2.417	-0.081
Ca1	-2.823	-1.087	-0.045	-2.827	-1.083	-0.043	-2.826	-1.084	-0.029
Ca2	-2.832	1.106	0.117	-2.830	1.108	0.121	-2.831	1.108	0.117
Ca3	-1.102	2.864	0.057	-1.100	2.860	0.059	-1.102	2.868	0.079
Ca4	1.084	2.857	-0.086	1.084	2.860	-0.087	1.086	2.858	-0.070
Ca5	2.826	1.092	0.004	2.831	1.091	0.005	2.834	1.096	-0.002
Ca6	2.839	-1.106	0.061	2.833	-1.106	0.081	2.835	-1.110	0.091
Ca7	1.101	-2.871	0.026	1.102	-2.873	0.012	1.106	-2.871	0.011
Ca8	-1.089	-2.859	-0.103	-1.085	-2.859	-0.105	-1.088	-2.863	-0.102

	Minimum			Extended			Complete		
Atom	x	y	z	x	y	z	x	y	z
Cb1	-4.202	-0.670	0.000	-4.207	-0.663	-0.013	-4.210	-0.656	-0.030
Cb2	-4.207	0.685	0.104	-4.207	0.692	0.097	-4.214	0.687	0.111
Cb3	-0.686	4.244	-0.072	-0.699	4.241	-0.061	-0.698	4.243	-0.071
Cb4	0.670	4.240	-0.173	0.656	4.242	-0.195	0.650	4.239	-0.194
Cb5	4.206	0.681	0.049	4.210	0.672	0.026	4.208	0.669	0.042
Cb6	4.215	-0.676	0.079	4.210	-0.685	0.076	4.202	-0.681	0.061
Cb7	0.676	-4.252	0.007	0.687	-4.254	0.015	0.679	-4.251	0.020
Cb8	-0.681	-4.244	-0.084	-0.670	-4.245	-0.097	-0.667	-4.251	-0.104

NSD Statistics

Table 24: Structure-cluster means of the minimum basis out-of-plane distortions from *Blastochloris viridis* RC cytochrome subunit hemes.

		Normal-mode displacement / Å					
		B2u	**B1u**	**A2u**	**Eg(x)**	**Eg(y)**	**A1u**
Cluster 1	**H1**	0.7232	0.1785	0.0337	0.1176	-0.0417	-0.0120
	H2	0.4395	0.3771	-0.0169	0.0765	-0.0500	-0.0088
	H3	0.4243	0.5478	-0.0235	0.0427	0.1342	0.0067
	H4	0.2267	0.1736	0.0112	0.0093	0.0759	0.0193
Cluster 2	**H1**	0.7504	0.2723	-0.1078	0.0922	-0.2141	-0.0148
	H2	0.4649	0.414	-0.1081	0.0149	-0.2328	0.0206
	H3	0.4430	0.6042	-0.1610	-0.1370	-0.1016	0.0107
	H4	0.2638	0.3107	-0.1797	0.0516	-0.0706	0.0105
Cluster 3	**H1**	0.4482	0.2969	0.0151	0.1519	0.0371	-0.0944
	H2	0.4428	0.5053	-0.0643	0.0878	-0.0864	0.0019
	H3	0.4102	0.4816	-0.0356	0.0717	0.0855	0.0045
	H4	0.2161	0.2937	0.0438	0.0185	0.1311	0.0277

H-NOx E_m / Q_{Fe} Calibration Curves

Table 25: Parameters of 2nd order polynomial obtained by least-squares fitting of H-NOx E_m data to calculated Q_{Fe}: - $E_m = a*Q_{Fe}^2 + b*Q_{Fe} + c$. a, b and c given as multiples of 10^3.

		Heme Diacid				FeP				FeP-comp				FeP-ext				FeP-min			
		a	*b*	*c*	R^2	*a*	*b*	*c*	R^2	*a*	*b*	*c*	R^2	*a*	*b*	*c*	R^2	*a*	*b*	*c*	R^2
Singlet	3-21g	-19.64	34.79	-15.23	0.96	-19.62	34.91	-15.35	0.90	-21.46	38.06	-16.70	0.96	-84.89	147.03	-63.50	0.81	-57.73	100.96	-43.97	0.79
	6-31g*																				
	6-311g**									13.40	-15.64	4.55	0.75								
	6-311+g**									-28.87	33.81	-9.73	0.96								
Triplet	3-21g	N/A	N/A	N/A	N/A	N/A	N/A	N/A	N/A	-1.27	2.69	-1.27	0.80	-0.29	0.68	0.17	0.48	3.40	-5.53	2.24	0.35
	6-31g*	25.16	-38.28	14.59	0.52	-17.99	30.48	-12.74	0.95	-18.13	30.70	-12.82	0.95	59.02	-89.38	33.83	0.72	-9.94	18.41	-8.26	0.77
	6-311g**	-40.49	53.42	-17.45	0.97	42.28	-51.37	15.64	0.60	-40.69	54.03	-17.76	0.96	191.47	-232.90	70.79	0.81	165.88	-201.81	61.38	0.84
	6-311+g**	N/A	N/A	N/A	N/A	-29.05	32.17	-8.74	0.96	-30.44	33.63	-9.12	0.97	-41.46	48.80	-14.07	0.80	2.86	1.78	-1.60	0.88

Table 26. Parameters of 2nd order polynomial obtained by least-squares fitting of H-NOx Em data to calculated NPA $Core_{Fe}$: - $Em = a* Core_{Fe}^2 + b* Core_{Fe} + c$.

		Heme Diacid				FeP				FeP-comp				FeP-ext				FeP-min			
		$a / 10^7$	$b / 10^8$	$c / 10^9$	R^2	$a / 10^7$	$b / 10^8$	$c / 10^9$	R^2	$a / 10^7$	$b / 10^8$	$c / 10^9$	R^2	$a / 10^7$	$b / 10^8$	$c / 10^9$	R^2	$a / 10^7$	$b / 10^8$	$c / 10^9$	R^2
Singlet	3-21g	-1.72	6.20	-5.58	0.95	-1.87	6.74	-6.06	0.92	-1.72	6.20	-5.58	0.97	-2.44	8.79	-7.91	0.78	-1.38	4.96	-4.46	0.77
	6-31g*																				
	6-311g**									-1.6	5.72	-5.1	0.96								
	6-311+g**									-0.92	3.30	-2.97	0.95								
Triplet	3-21g																				
	6-31g*	-1.98	7.11	-6.39	0.96	-1.83	6.59	-5.93	0.96	-1.85	6.64	-5.97	0.97	-6.08	21.9	-19.7	0.81	-1.80	6.47	-5.82	0.81
	6-311g**	-1.99	7.17	-6.45	0.97	-2.41	8.66	-7.79	0.95	-2.07	7.44	-6.69	0.97	-3.99	14.4	-12.9	0.84	0.39	-1.40	1.26	0.81
	6-311+g**	N/A	N/A	N/A	N/A	-1.33	4.79	-4.31	0.96	-1.36	4.89	-4.40	0.97	-2.45	8.82	-7.93	0.84	-1.20	4.30	-3.87	0.87

Table 27. Parameters of linear fits obtained by the method of least-squares of H-NOx Em data (excluding 1U56 structures) to calculated NPA $Core_{Fe}$: - $Em = a* Core_{Fe} + b$.

		Heme Diacid			FeP			FeP-comp			FeP-ext			FeP-min		
		$a / 10^4$	$b / 10^6$	R^2	$a / 10^4$	$b / 10^6$	R^2	$a / 10^4$	$b / 10^6$	R^2	$a / 10^4$	$b / 10^6$	R^2	$a / 10^4$	$b / 10^6$	R^2
Singlet	3-21g	-9.22	1.66	0.88	-9.24	1.66	0.79	-9.38	1.69	0.93	-9.45	1.70	0.87	-8.97	1.61	0.82
	6-31g*															
	6-311g**							-8.39	1.51	0.88						
	6-311+g**							-6.92	1.24	0.92						
Triplet	3-21g	-10.5	1.89	0.84				-9.78	1.76	0.89	-8.04	1.45	0.91	-10.3	1.85	0.89
	6-31g*	-6.23	1.12	0.89	-6.16	1.11	0.88	-6.19	1.11	0.90	-10.3	1.85	0.86	-7.79	1.40	0.88
	6-311g**	-9.95	1.79	0.92	-9.93	1.79	0.91	-10.0	1.80	0.95	-12.1	2.18	0.83	-9.19	1.65	0.72
	6-311+g**	N/A	N/A	N/A	-8.07	1.45	0.91	-8.06	1.45	0.94	-9.11	1.64	0.85	-8.31	1.50	0.90

Comparison of Q_{Fe} and NPA $Core_{Fe}$ from structural models of decreasing complexity

Table 28. Parameters of linear fits obtained by the method of least-squares of H-NOx diacid $Q_{Fe\text{-}MBS}$ against the various reduced models.

		FeP			FeP-comp			FeP-ext*			FeP-min*		
		a	*b*	R^2	*a*	*b*	R^2	*a*	*b*	R^2	*a*	*b*	R^2
Singlet	3-21g	1.03	-0.03	0.97	1.06	-0.05	0.99	1.91	-0.78	0.68	1.69	-0.59	0.66
Triplet	3-21g												
	6-31g*#	0.57	0.32	0.26	0.56	0.33	0.25	-0.80	1.38	0.45	0.97	0.00	0.41
	6-311g**#	0.29	0.44	0.10	1.06	-0.04	0.99	3.09	-1.33	0.81	1.62	-0.40	0.65

Table 29. Parameters of linear fits obtained by the method of least-squares of H-NOx diacid $Q_{Fe\text{-}MBS}$ against the various reduced models excluding the 1U56-B.

		FeP			FeP-comp			FeP-ext*			FeP-min*		
		a	*b*	R^2	*a*	*b*	R^2	*a*	*b*	R^2	*a*	*b*	R^2
Singlet	3-21g	0.99	0.01	0.96	1.02	-0.02	1.00	1.79	-0.69	0.91	1.57	-0.49	0.86
Triplet	3-21g												
	6-31g*#	1.02	-0.02	1.00	1.03	-0.02	1.00	-0.68	1.29	0.44	1.22	-0.19	0.88
	6-311g**#	1.00	0.00	1.00	1.00	-0.01	1.00	2.80	-1.15	0.79	1.42	-0.28	0.62

Table 30. Parameters of linear fits obtained by the method of least-squares of H-NOx diacid $Q_{Fe\text{-}MBS}$ against the various reduced models excluding the 1U56 structures.

		FeP			FeP-comp			FeP-ext*			FeP-min*		
		a	*b*	R^2	*a*	*b*	R^2	*a*	*b*	R^2	*a*	*b*	R^2
Singlet	3-21g	1.01	-0.01	0.86	1.06	-0.05	0.99	1.31	-0.29	0.89	1.09	-0.10	0.73
Triplet	3-21g												
	6-31g*#	1.01	-0.01	0.99	1.01	-0.01	0.99	1.07	-0.08	0.74	0.83	0.12	0.71
	6-311g**#	0.99	0.00	0.98	0.99	0.00	0.99	1.52	-0.35	0.61	0.72	0.16	0.61

Table 31. Parameters of linear fits obtained by the method of least-squares of H-NOx FeP $Q_{Fe\text{-}MBS}$ against the various reduced models.

		FeP-comp			FeP-ext*			FeP-min*		
		a	*b*	R^2	*a*	*b*	R^2	*a*	*b*	R^2
Singlet	3-21g	1.01	-0.01	0.98	1.80	-0.68	0.65	1.59	-0.50	0.63
Triplet	3-21g									
	6-31g*#	1.00	0.00	1.00	-0.51	1.17	0.22	1.27	-0.23	0.85
	6-311g**#	0.49	0.31	0.18	1.49	-0.33	0.16	0.80	0.11	0.13
	6-311+g**	1.05	-0.02	0.99	2.37	-0.72	0.75	1.84	-0.44	0.79

Table 32. Parameters of linear fits obtained by the method of least-squares of H-NOx FeP $Q_{Fe\text{-}MBS}$ against the various reduced models excluding the 1U56-B.

		FeP-comp			FeP-ext*			FeP-min*		
		a	*b*	R^2	*a*	*b*	R^2	*a*	*b*	R^2
Singlet	3-21g	1.00	0.00	0.97	1.69	-0.60	0.82	1.48	-0.42	0.78
Triplet	3-21g									
	6-31g*#	1.01	-0.01	1.00	-0.66	1.28	0.44	1.20	-0.17	0.88
	6-311g**#	1.01	0.00	1.00	2.77	-1.13	0.77	1.44	-0.28	0.63
	6-311+g**	1.01	0.00	1.00	2.16	-0.62	0.79	1.68	-0.36	0.81

Table 33. Parameters of linear fits obtained by the method of least-squares of H-NOx FeP $Q_{Fe\text{-}MBS}$ against the various reduced models excluding the 1U56 structures.

		FeP-comp			FeP-ext*			FeP-min*		
		a	*b*	R^2	*a*	*b*	R^2	*a*	*b*	R^2
Singlet	3-21g	0.93	0.06	0.89	1.06	-0.08	0.69	0.87	0.08	0.54
Triplet	3-21g									
	6-31g*#	1.00	0.00	1.00	1.05	-0.06	0.74	0.82	0.12	0.72
	6-311g**#	0.99	0.01	0.99	1.46	-0.31	0.57	0.74	0.15	0.65
	6-311+g**	0.99	0.00	0.99	1.21	-0.13	0.72	0.99	-0.01	0.88

Table 34. Parameters of linear fits obtained by the method of least-squares of H-NOx diacid NPA $Core_{Fe}$ against the various reduced models.

		FeP			FeP-comp			FeP-ext*			FeP-min*		
		a	*b*	R^2	*a*	*b*	R^2	*a*	*b*	R^2	*a*	*b*	R^2
Singlet	3-21g	1.08	-1.40	0.99	1.08	-1.39	0.99	1.53	-9.52	0.71	1.48	-8.72	0.73
Triplet	3-21g												
	6-31g*#	0.96	0.80	1.00	0.95	0.86	0.99	1.54	-9.76	0.74	1.28	-5.06	0.91
	6-311g**#	1.07	-1.22	0.96	1.02	-0.27	0.99	1.86	-15.39	0.84	1.52	-9.45	0.83

Table 35. Parameters of linear fits obtained by the method of least-squares of H-NOx diacid NPA $Core_{Fe}$ against the various reduced models excluding the 1U56 structures.

		FeP			FeP-comp			FeP-ext*			FeP-min*		
		a	*b*	R^2	*a*	*b*	R^2	*a*	*b*	R^2	*a*	*b*	R^2
Singlet	3-21g	1.04	-0.74	0.97	0.98	0.29	0.99	1.01	-0.09	0.96	0.96	0.72	0.91
Triplet	3-21g				0.90	1.84	0.99	0.66	6.05	0.82	0.89	2.01	0.87
	6-31g*#	1.00	0.01	1.00	0.99	0.23	0.99	0.93	1.29	0.92	0.96	0.71	0.90
	6-311g**#	1.00	-0.04	1.00	0.99	0.20	0.99	1.22	-3.88	0.89	0.96	0.78	0.84

Table 36. Parameters of linear fits obtained by the method of least-squares of H-NOx FeP NPA $Core_{Fe}$ against the various reduced models.

		FeP-comp			FeP-ext*			FeP-min*		
		a	*b*	R^2	*a*	*b*	R^2	*a*	*b*	R^2
Singlet	3-21g	0.99	0.13	0.99	1.43	-7.73	0.72	1.39	-6.99	0.75
Triplet	3-21g									
	6-31g*#	1.00	0.06	1.00	1.58	-10.48	0.72	1.31	-5.64	0.88
	6-311g**#	0.93	1.32	0.98	1.77	-13.90	0.90	1.44	-8.00	0.88
	6-311+g**	0.89	1.98	0.98	1.72	-13.00	0.83	1.52	-9.37	0.86

Table 37. Parameters of linear fits obtained by the method of least-squares of H-NOx FeP NPA $Core_{Fe}$ against the various reduced models excluding the 1U56 structures.

		FeP-comp			FeP-ext*			FeP-min*		
		a	*b*	R^2	*a*	*b*	R^2	*a*	*b*	R^2
Singlet	3-21g	0.90	1.74	0.93	0.91	1.70	0.87	0.87	2.34	0.84
Triplet	3-21g									
	6-31g*#	0.99	0.23	0.99	0.93	1.31	0.92	0.96	0.72	0.90
	6-311g**#	0.99	0.26	0.99	1.21	-3.80	0.89	0.95	0.83	0.84
	6-311+g**	0.97	0.46	0.99	1.11	-1.94	0.90	1.00	-0.02	0.93

Cofactor NSDs

H-NOx

Table 38: Normal-mode displacements, total distortions and goodness-of-fits from the minimum basis NSD of the hemes from the H-NOx crystal structures.

Cofactor ID	Dip	δip	B2g	B1g	Eu(x)	Eu(y)	A1g	A2g	Doop	δoop	B2u	B1u	A2u	Eg(x)	Eg(y)	A1u
1u56 - A500	0.1950	0.0265	0.0133	0.0789	-0.0422	-0.0735	-0.1564	-0.0002	1.6329	0.0284	-1.1147	-1.1707	-0.1531	0.0190	0.1708	-0.0163
1u56 - B501	0.0849	0.0168	-0.0332	0.0654	-0.0284	0.0227	0.0227	-0.0024	1.0173	0.0214	-0.7111	-0.5538	0.2050	-0.4232	0.0344	-0.0185
3eee - A200	0.1873	0.0290	0.0085	-0.0515	0.0575	0.0873	0.1462	0.0075	0.8809	0.0280	-0.3969	-0.7660	0.0417	-0.1727	0.0151	0.0044
3eee - B200	0.2642	0.0296	0.0937	-0.0336	0.0684	0.0729	0.2232	0.0084	0.8001	0.0285	-0.5017	-0.6115	0.0282	-0.1130	-0.0312	0.0075
3eee - C200	0.2518	0.0260	-0.0542	0.0538	0.0466	0.0308	0.2333	-0.0010	0.5290	0.0144	-0.0431	-0.4876	-0.0940	-0.1587	0.0778	0.0123
3eee - D200	0.2623	0.0258	-0.0686	0.0790	0.0900	0.0695	0.2120	-0.0036	0.6072	0.0213	0.0667	-0.5166	-0.0253	-0.2506	-0.1839	0.0078
3nvr - A200	0.2540	0.0367	-0.2443	0.0455	-0.0051	0.0512	-0.0043	0.0106	1.1383	0.0421	-0.8358	-0.6344	0.1590	-0.3384	0.2341	0.0060
3nvr - B200	0.1639	0.0317	-0.1436	0.0496	-0.0162	0.0560	-0.0186	0.0068	1.1572	0.0431	-0.8206	-0.7585	0.0694	-0.2650	0.1245	0.0015
3nvu - A200	0.2656	0.0245	-0.2154	-0.0658	0.0571	0.0598	0.1133	0.0130	0.6352	0.0288	-0.4505	-0.2164	0.1114	-0.3743	0.0334	-0.0001

3nvu - B200	0.1204	0.0252	0.0099	-0.0194	0.0458	0.0088	0.1086	-0.0070	0.5597	0.0183	-0.4167	-0.2611	0.0516	-0.2561	-0.0560	0.0071

Blastochloris viridis RC cytochrome subunit

Table 39: Normal-mode displacements, total distortions and goodness-of-fits from the minimum basis NSD of the hemes from the *B. viridis* RC crystal structures.

Cofactor ID	Dip	δip	B2g	B1g	Eu(x)	Eu(y)	A1g	A2g	Doop	δoop	B2u	B1u	A2u	Eg(x)	Eg(y)	A1u
1dxr - C401	0.1875	0.0108	-0.0976	0.0940	0.0643	0.0377	0.1060	0.0034	0.6092	0.0270	0.4922	0.2840	0.0285	0.1914	0.0581	-0.0862
1dxr - C402	0.2131	0.0079	-0.1061	-0.0396	0.0100	-0.0051	0.1802	0.0028	0.6137	0.0240	0.4316	0.4214	-0.0324	0.0744	-0.0734	0.0282
1dxr - C403	0.1341	0.0091	0.0320	0.0743	0.0246	-0.0674	0.0793	-0.0003	0.6455	0.0211	0.3600	0.5293	-0.0332	0.0476	0.0587	0.0045
1dxr - C404	0.2132	0.0095	-0.1431	-0.0827	0.0312	0.0404	0.1244	0.0070	0.3296	0.0115	0.2194	0.1712	0.0419	0.0511	0.1600	0.0346
1prc - C609	0.3751	0.0353	-0.2737	0.0784	0.0361	0.1588	-0.1819	0.0079	0.7061	0.0247	0.6342	0.2592	0.1402	0.0393	-0.0752	0.0486
1prc - C610	0.2937	0.0391	-0.1012	0.1901	-0.0871	0.0096	-0.1778	-0.0242	0.5571	0.0199	0.3933	0.3796	0.0446	0.0408	-0.0813	0.0351
1prc - C611	0.2127	0.0280	-0.1254	-0.1184	0.0398	-0.0266	-0.1138	0.0166	0.6687	0.0260	0.5126	0.4061	0.0067	0.0792	0.1146	-0.0012
1prc - C612	0.1583	0.0309	0.1075	-0.1105	-0.0069	-0.0144	0.0156	0.0283	0.2829	0.0142	0.1729	0.0305	0.1135	0.1024	0.1561	-0.0383
1r2c - C1201	0.0943	0.0072	-0.0355	0.0312	0.0074	0.0099	0.0805	0.0042	0.8362	0.0334	0.8235	0.0979	-0.0640	0.0708	-0.0388	-0.0296
1r2c - C1202	0.0615	0.0088	-0.0029	0.0124	0.0036	-0.0107	0.0589	-0.0050	0.5873	0.0317	0.4381	0.3557	-0.1171	0.0973	0.0030	-0.0570
1r2c - C1203	0.1097	0.0074	-0.0487	0.0707	0.0600	-0.0128	0.0299	-0.0021	0.6395	0.0217	0.3436	0.4917	-0.0176	0.0539	0.2143	0.0062
1r2c - C1204	0.0953	0.0073	0.0203	-0.0323	0.0364	0.0115	0.0784	0.0036	0.2664	0.0201	0.1534	0.2009	-0.0381	0.0352	0.0494	0.0438
1vrn - C401	0.1444	0.0071	-0.0627	0.0254	0.0091	-0.0049	0.1272	-0.0001	0.6819	0.0247	0.6578	0.1247	0.0846	0.0733	0.0421	-0.0488
1vrn - C402	0.1260	0.0052	-0.0188	0.0025	0.0081	-0.0144	0.1235	0.0030	0.5558	0.0177	0.4070	0.3724	0.0449	0.0165	-0.0484	-0.0024
1vrn - C403	0.1085	0.0066	0.0594	0.0221	0.0310	0.0067	0.0821	0.0027	0.7133	0.0202	0.4035	0.5831	-0.0119	0.0029	0.0719	0.0236
1vrn - C404	0.1419	0.0053	-0.0684	-0.0205	0.0239	-0.0165	0.1191	0.0028	0.3760	0.0176	0.2334	0.2701	0.0617	-0.0355	0.0828	0.0453
2i5n - C401	0.2504	0.0180	-0.0995	0.0391	0.0053	-0.0128	0.2259	0.0069	0.7956	0.0356	0.7645	0.1058	-0.0476	0.0904	-0.1636	-0.0042
2i5n - C402	0.2271	0.0159	-0.0518	-0.0538	0.0134	-0.0201	0.2127	0.0129	0.5792	0.0261	0.4073	0.3324	-0.0899	0.0389	-0.2182	0.0433
2i5n - C403	0.2011	0.0169	0.0109	-0.0322	-0.0011	0.0126	0.1972	0.0159	0.7404	0.0277	0.4417	0.5482	-0.1733	-0.0793	-0.1179	0.0477
2i5n - C404	0.2446	0.0157	-0.0431	-0.0560	0.0217	-0.0201	0.2317	0.0167	0.4576	0.0141	0.3140	0.3018	-0.1055	0.0219	-0.0886	0.0144
2jbl - C1333	0.1266	0.0067	-0.0305	0.0336	0.0186	-0.0082	0.1163	0.0042	0.5839	0.0247	0.4774	0.2869	0.0809	0.0976	0.0389	-0.1146
2jbl - C1334	0.1521	0.0070	-0.0535	-0.0515	0.0155	-0.0002	0.1318	0.0003	0.6238	0.0284	0.4266	0.4369	-0.0792	0.0718	-0.0591	-0.0356
2jbl - C1335	0.1247	0.0063	0.0748	-0.0163	0.0177	-0.0037	0.0967	0.0016	0.5901	0.0345	0.4036	0.4170	-0.0309	-0.0197	0.0987	-0.0175
2jbl - C1336	0.1353	0.0071	0.0554	-0.0630	-0.0192	0.0092	0.1039	0.0032	0.4891	0.0277	0.3281	0.3362	-0.0595	0.0889	0.0668	-0.0517
2prc - C337	0.1688	0.0098	-0.1150	0.0423	0.0679	-0.0084	0.0938	0.0028	0.5119	0.0316	0.3981	0.2650	-0.0205	0.1457	0.0771	-0.0756
2prc - C338	0.2440	0.0138	-0.1902	-0.0441	0.0009	-0.0168	0.1452	0.0084	0.7621	0.0231	0.4376	0.5972	-0.1036	0.0529	-0.1378	0.0071
2prc - C339	0.1256	0.0107	0.0008	0.0060	-0.0003	-0.0616	0.1092	0.0055	0.6141	0.0398	0.4580	0.3650	-0.0724	0.1350	0.0990	-0.0285
2prc - C340	0.1519	0.0069	0.0409	-0.0804	0.0572	-0.0003	0.1079	0.0050	0.3082	0.0323	0.1810	0.2215	-0.0047	-0.0030	0.1099	0.0320

Cofactor ID	Dip	δip	B2g	B1g	Eu(x)	Eu(y)	A1g	A2g	Doop	δoop	B2u	B1u	A2u	Eg(x)	Eg(y)	A1u
2wjm - C1333	0.2051	0.0303	-0.0648	-0.0295	0.0595	0.0548	0.1740	-0.0141	0.8110	0.0337	0.7604	0.1926	-0.0075	0.2047	-0.0233	-0.0046
2wjm - C1334	0.2684	0.0263	-0.1586	0.1395	0.0351	-0.0431	0.1555	0.0108	0.5856	0.0244	0.4573	0.3450	-0.0227	0.1114	-0.0434	0.0017
2wjm - C1335	0.2517	0.0296	-0.0654	0.0183	0.1286	-0.0124	0.1957	0.0612	0.7690	0.0287	0.4293	0.6100	-0.0469	0.0477	0.1743	0.0111
2wjm - C1336	0.2046	0.0267	0.0359	0.1730	0.0076	0.0205	0.1009	-0.0002	0.3521	0.0112	0.2923	0.1766	-0.0320	-0.0671	0.0369	0.0219
2wjn - C1333	0.3271	0.0326	-0.2315	-0.0474	0.0475	0.0327	0.2184	-0.0125	0.8057	0.0346	0.7403	0.2182	0.0154	0.1998	-0.1133	-0.0254
2wjn - C1334	0.4712	0.0342	-0.3633	0.0513	-0.0119	-0.0872	0.2822	0.0036	0.6789	0.0262	0.5018	0.4330	-0.0344	0.1166	-0.0799	-0.0215
2wjn - C1335	0.2547	0.0352	-0.1241	0.0439	0.1159	-0.0267	0.1827	-0.0037	0.7872	0.0305	0.4325	0.6482	-0.0477	0.0300	0.0960	-0.0061
2wjn - C1336	0.1756	0.0359	-0.1235	0.0864	-0.0162	0.0469	0.0747	-0.0082	0.3483	0.0115	0.2813	0.1901	-0.0493	0.0115	0.0544	0.0236
3d38 - C401	0.1481	0.0235	-0.0292	0.0666	-0.0455	-0.0010	0.1186	0.0228	1.0011	0.0528	0.7496	0.5248	-0.1898	0.1618	-0.3181	-0.0381
3d38 - C402	0.1438	0.0219	-0.0084	-0.0857	-0.0180	-0.0236	0.1067	0.0312	0.9274	0.0414	0.5899	0.6032	-0.1720	-0.0027	-0.3444	0.0110
3d38 - C403	0.1542	0.0214	0.0740	0.0533	-0.0221	-0.0387	0.1155	0.0118	0.8613	0.0298	0.4411	0.6773	-0.1882	-0.1994	-0.1139	-0.0195
3d38 - C404	0.1243	0.0176	0.0323	-0.0385	-0.0084	0.0289	0.1077	0.0206	0.5279	0.0218	0.1519	0.3797	-0.3039	0.1154	-0.0756	0.0106
3g7f - C401	0.1498	0.0171	-0.0659	0.0159	0.0012	0.0140	0.1325	0.0097	0.7822	0.0361	0.7370	0.1863	-0.0861	0.0245	-0.1607	-0.0020
3g7f - C402	0.2089	0.0127	0.0231	-0.0875	-0.0038	0.0138	0.1876	0.0069	0.5239	0.0235	0.3976	0.3064	-0.0623	0.0085	-0.1359	0.0076
3g7f - C403	0.1780	0.0148	0.0404	-0.0931	0.0190	0.0259	0.1392	0.0312	0.7624	0.0252	0.4462	0.5870	-0.1216	-0.1324	-0.0729	0.0040
3g7f - C404	0.1618	0.0169	0.0509	-0.0714	0.0303	0.0175	0.1309	0.0104	0.4337	0.0198	0.3254	0.2506	-0.1296	0.0174	-0.0477	0.0066
3prc - C337	0.2056	0.0098	-0.1203	0.0895	0.0841	0.0059	0.1124	0.0060	0.6438	0.0264	0.4621	0.4203	-0.0288	0.0737	0.0957	-0.0939
3prc - C338	0.1708	0.0092	0.0413	-0.0441	-0.0041	-0.0341	0.1559	-0.0068	0.6416	0.0309	0.3912	0.4717	-0.0883	0.0712	-0.1512	-0.0193
3prc - C339	0.0858	0.0103	0.0368	0.0209	-0.0117	-0.0723	0.0141	-0.0014	0.6904	0.0227	0.4091	0.5398	0.0132	0.1168	0.0641	-0.0020
3prc - C340	0.1153	0.0082	-0.0514	-0.0683	0.0135	0.0111	0.0753	0.0041	0.4039	0.0217	0.2075	0.2804	0.0417	-0.0024	0.1800	0.0854
5prc - C337	0.1379	0.0093	-0.0317	0.0951	0.0748	0.0210	0.0537	0.0061	0.5067	0.0288	0.4395	0.1697	0.0172	0.1562	0.0195	-0.0988
5prc - C338	0.2207	0.0095	-0.1935	-0.0324	-0.0222	0.0301	0.0939	0.0002	0.6814	0.0298	0.4796	0.4567	-0.0434	0.1282	-0.0785	0.0347
5prc - C339	0.1230	0.0104	-0.0826	0.0681	-0.0086	-0.0487	0.0345	-0.0069	0.6768	0.0308	0.4190	0.5107	0.0032	0.0519	0.1305	0.0449
5prc - C340	0.1384	0.0090	-0.0668	-0.0934	0.0240	0.0255	0.0683	0.0083	0.3714	0.0223	0.1996	0.2377	0.1432	-0.0240	0.1376	0.0400
6prc - C337	0.1544	0.0079	-0.0586	0.1109	0.0559	0.0175	0.0680	0.0077	0.5292	0.0317	0.3857	0.2834	0.0189	0.2039	0.0145	-0.0940
6prc - C338	0.2012	0.0104	-0.1682	0.0105	-0.0259	0.0015	0.1067	0.0057	0.6912	0.0284	0.4200	0.5327	-0.0607	0.0940	-0.0701	0.0084
6prc - C339	0.1001	0.0093	-0.0720	0.0106	0.0275	-0.0602	0.0178	-0.0039	0.7102	0.0215	0.4113	0.5645	-0.0257	0.0440	0.1168	0.0152
6prc - C340	0.1467	0.0106	-0.0822	-0.0447	0.0227	0.0175	0.1094	-0.0015	0.3841	0.0225	0.2065	0.2784	0.1059	0.0249	0.1231	0.0202
7prc - C337	0.1749	0.0119	-0.1073	0.1177	0.0708	0.0079	0.0100	0.0057	0.6470	0.0378	0.4827	0.3688	0.0092	0.1946	-0.0439	-0.0979
7prc - C338	0.1707	0.0125	-0.1272	-0.1018	-0.0419	-0.0098	0.0266	-0.0049	0.8159	0.0323	0.5128	0.6203	-0.0424	0.1220	-0.0350	-0.0103
7prc - C339	0.0843	0.0104	-0.0547	0.0553	0.0170	-0.0255	0.0101	-0.0050	0.6276	0.0259	0.4103	0.4447	-0.1036	0.1261	0.0310	0.0149
7prc - C340	0.1758	0.0165	-0.0639	-0.1165	-0.0250	-0.0048	0.1117	-0.0125	0.5773	0.0315	0.1707	0.5307	0.0384	-0.0061	0.1406	0.0335

References

(Complete Reference 33) Frisch, M. J.; Trucks, G. W.; Schlegel, H. B.; Scuseria, G. E.; Robb, M. A.; Cheeseman, J. R.; Scalmani, G.; Barone, V.; Mennucci, B.; Petersson, G. A.; Nakatsuji, H.; Caricato, M.; Li, X.; Hratchian, H. P.; Izmaylov, A. F.; Bloino, J.; Zheng, G.; Sonnenberg, J. L.; Hada, M.; Ehara, M.; Toyota, K.; Fukuda, R.; Hasegawa, J.; Ishida, M.; Nakajima, T.; Honda, Y.; Kitao, O.; Nakai, H.; Vreven, T.; Montgomery, J., J. A.; Peralta, J. E.; Ogliaro, F.; Bearpark, M.; Heyd, J. J.; Brothers, E.; Kudin, K. N.; Staroverov, V. N.; Kobayashi, R.; Normand, J.; Raghavachari, K.; Rendell, A.; Burant, J. C.; Iyengar, S. S.; Tomasi, J.; Cossi, M.; Rega, N.; Millam, N. J.; Klene, M.; Knox, J. E.; Cross, J. B.; Bakken, V.; Adamo, C.; Jaramillo, J.; Gomperts, R.; Stratmann, R. E.; Yazyev, O.; Austin, A. J.; Cammi, R.; Pomelli, C.; Ochterski, J. W.; Martin, R. L.; Morokuma, K.; Zakrzewski, V. G.; Voth, G. A.; Salvador, P.; Dannenberg, J. J.; Dapprich, S.; Daniels, A. D.; Farkas, Ö.; Foresman, J. B.; Ortiz, J. V.; Cioslowski, J.; Fox, D. J. Gaussian 09, Revision A. 02, Gaussian, Inc.: Wallin[45] C. R. Lancaster, M. V. Bibikova, P. Sabatino, D. Oesterhelt, H. Michel, J Biol Chem 2000, 275, 39364-39368.

1. J. Deisenhofer, O. Epp, I. Sinning, H. Michel, J Mol Biol 1995, 246, 429-457.

2. R. H. Baxter, N. Ponomarenko, V. Srajer, R. Pahl, K. Moffat, J. R. Norris, Proc Natl Acad Sci U S A 2004, 101, 5982-5987.

3. R. H. Baxter, B. L. Seagle, N. Ponomarenko, J. R. Norris, Acta Crystallogr D Biol Crystallogr 2005, 61, 605-612.

4. L. Li, D. Mustafi, Q. Fu, V. Tereshko, D. L. Chen, J. D. Tice, R. F. Ismagilov, Proc Natl Acad Sci U S A 2006, 103, 19243-19248.

5. C. R. Lancaster, C. Hunte, J. Kelley, 3rd, B. L. Trumpower, R. Ditchfield, J Mol Biol 2007, 368, 197-208.

6. C. R. Lancaster, H. Michel, Structure 1997, 5, 1339-1359.

7. A. B. Wohri, W. Y. Wahlgren, E. Malmerberg, L. C. Johansson, R. Neutze, G. Katona, Biochemistry 2009, 48, 9831-9838.

8. L. Li, S. Nachtergaele, A. M. Seddon, V. Tereshko, N. Ponomarenko, R. F. Ismagilov, J Am Chem Soc 2008, 130, 14324-14328.

9. N. S. Ponomarenko, L. Li, A. R. Marino, V. Tereshko, A. Ostafin, J. A. Popova, E. J. Bylina, R. F. Ismagilov, J. R. Norris, Jr., Biochim Biophys Acta 2009, 1788, 1822-1831.

10. C. R. Lancaster, H. Michel, J Mol Biol 1999, 286, 883-898.gford CT, 2009.

Table of Figures

List of Tables